Inorganic Chemistry

Award Paper

pubs.acs.org/IC

Development of Molecular Electrocatalysts for Energy Storage

Daniel L. DuBois*

Center for Molecular Electrocatalysis, Chemical and Materials Sciences Division, Pacific Northwest National Laboratory, P.O. Box 999, K2-57, Richland, Washington 99352, United States

ABSTRACT: Molecular electrocatalysts can play an important role in energy storage and utilization reactions needed for intermittent renewable energy sources. This manuscript describes three general themes that our laboratories have found useful in the development of molecular electrocatalysts for reduction of CO_2 to CO and for H_2 oxidation and production. The first theme involves a conceptual partitioning of catalysts into first, second, and outer coordination spheres. This is illustrated with the design of electrocatalysts for CO_2 reduction to CO using first and second coordination spheres and for H_2 production catalysts using all three coordination spheres. The second theme focuses on the development of thermodynamic models that can be used to design catalysts to avoid high- and low-energy intermediates. In this research, new approaches to the measurement of thermodynamic hydride donor and acceptor abilities of transition-metal complexes were developed. Combining this information with other thermodynamic information such as pK_a values and redox potentials led to more complete thermodynamic descriptions of transition-metal hydride, dihydride, and related species. Relationships extracted from this information were then used to develop models that are powerful tools for predicting and understanding the relative free energies of intermediates in catalytic reactions. The third theme is control of proton movement during electrochemical fuel generation and utilization reactions. This research involves the incorporation of pendant amines in the second coordination sphere that can facilitate H−H bond heterolysis and heteroformation, intra- and intermolecular proton-transfer steps, and coupling of proton- and electron-transfer steps. Studies also indicate an important role for the outer coordination sphere in the delivery of protons to the second coordination sphere. Understanding these proton-transfer reactions and their associated energy barriers is key to the design of faster and more efficient molecular electrocatalysts for energy storage.

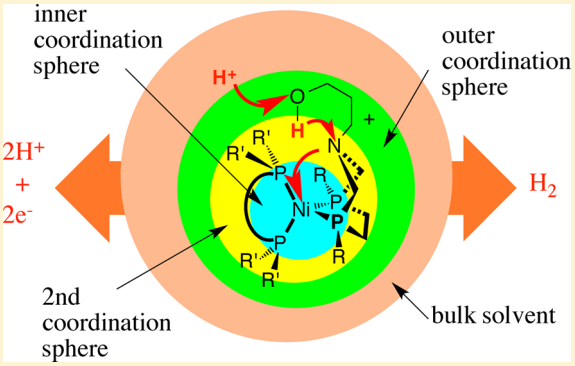

INTRODUCTION

The development of fast, efficient, inexpensive, and durable electrocatalysts for interconversion of electrical energy and fuels will be essential for the widespread use of wind and solar energy.[1] Both of these renewable energy sources can contribute significantly to our energy needs, but their energy output can vary over periods as short as a few minutes to as long as a year. This leads to mismatches between energy production and demand that could be overcome by energy storage. An attractive strategy for energy storage is the electrochemical reduction of H_2O, CO_2, N_2, and other abundant substrates to fuels, as shown in Figure 1. These reactions take place at the cathode of an electrolysis or photoelectrochemical cell, and a corresponding oxidation process, generally oxidation of water to produce O_2, must occur at the anode. The electrocatalysts for both the cathodic and anodic processes must be extremely efficient to avoid severe energy losses during the production of fuels. Similar constraints apply to electrocatalysts used in fuel cells, which are needed for the efficient generation of electricity upon demand.

This perspective outlines three general themes or concepts that have proven useful in our research for developing molecular electrocatalysts for CO_2 reduction, H_2 production and oxidation, formate oxidation, and O_2 reduction. These

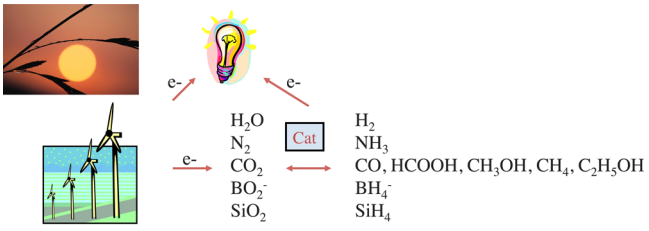

Figure 1. Possible energy storage reactions using abundant substrates.

three themes are (1) the conceptual breaking of the structure of a catalyst into first, second, and outer coordination spheres (a modular approach),[2] (2) an energy-based approach in which thermodynamic relationships are used to predict and control the energies of catalytic intermediates, and (3) control of the proton movement within and between the different coordination spheres.

In our definition of a modular approach, the first coordination sphere consists of the metal center of interest and the atoms bonded directly to it. The second coordination sphere includes functional groups incorporated in the ligand

Received: October 26, 2013
Published: February 20, 2014

   dx.doi.org/10.1021/ic4026969 | *Inorg. Chem.* 2014, 53, 3935−3960

structure that can interact directly with substrates bound to the metal during a catalytic cycle but that interact very weakly, or not at all, with the metal center. The outer coordination sphere consists of the remainder of the ligand structure and the solvent immediately surrounding the catalyst. Catalyst evolution is achieved by optimizing each coordination sphere for the specific functions that they perform and the different coordination spheres with each other.

The energy-based aspect of the modular energy-based approach arises from consideration of the properties of an ideal catalyst. Figure 2 shows hypothetical reaction profiles for the reduction of two protons to H_2 via an uncatalyzed pathway (solid black line), a pathway involving a catalyst with high- and low-energy intermediates (blue barriers and red intermediates), and a pathway corresponding to an ideal catalyst (purple barriers and blue intermediates). For an ideal catalyst, high- and low-energy intermediates that contribute to large activation barriers are avoided. As an example, the rapid and reversible oxidation of H_2 by the active site of the [FeFe]hydrogenase enzyme implies that the free energy of the overall reaction is close to 0 kcal/mol and that the free energies of the H_2 complex, **1**, and the product of heterolytic cleavage of H_2, **2**, are also nearly the same.[3] For the ideal catalyst shown in Figure 2, the intrinsic activation barriers are also low. Thus, the design of a catalyst with performance characteristics approaching those of an ideal catalyst implies the ability to control the relative energies of all of the intermediates of a catalytic cycle. This, in turn, requires an understanding of the factors that determine the relative free energies of these catalytic intermediates and the development of predictive quantitative models. In the following discussion, efforts will be made to illustrate both the modular- and energy-based aspects of catalyst design.

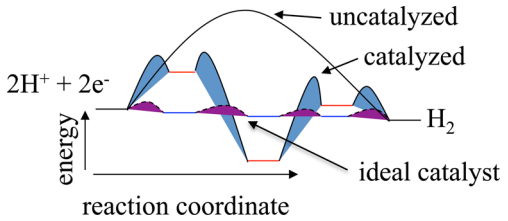

Figure 2. Hypothetical reaction profiles for the catalytic reduction of protons to H_2 showing a large barrier associated with uncatalyzed reduction (solid black line), smaller barriers for a catalyzed reaction (blue profile), and finally a profile that would represent an ideal catalytic process (purple profile).

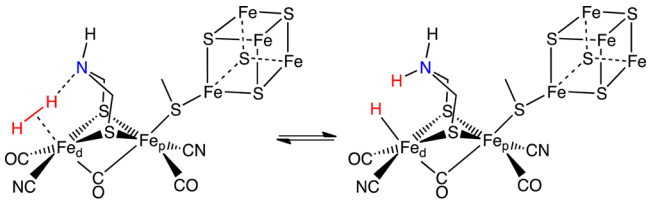

1 **2**

A third theme of our research has been the control of proton movement during electrocatalytic reactions. All of the fuel generation reactions shown in Figure 1 require multiple protons as well as electrons. Proton transfer is much less facile than electron transfer because a proton is approximately 2000 times as massive as an electron. Fast electron-transfer reactions can occur over distances of 10 Å or more. For example, the average distance between $[Fe_4S_4]$ clusters in hydrogenase enzymes is 12 Å.[3] However, proton-transfer reactions typically occur over very short distances, with the proton actually moving less than 1 Å.[4] The low-energy barriers shown in Figure 2 for an ideal catalyst imply very precise control of the movement of protons. In the hydrogenase enzyme, it is thought that the proton shown in the exo position of the pendant amine with respect to the distal iron (Fe_d) of **2** is transferred to a proton conduction channel in the outer coordination sphere, which facilitates proton exchange with acids and bases in solution.[3b] In the third section of this manuscript, the electrocatalytic oxidation and production of H_2 provides an ideal reaction for studying changes in the H−H distances from 0.74 to 10 Å or more. This proton movement is facilitated by the presence of pendant bases and acids in the second coordination sphere as well as a properly designed outer coordination sphere.

MODULAR APPROACH TO MOLECULAR ELECTROCATALYSTS FOR CO_2 REDUCTION

Optimization of the First Coordination Sphere. Both electrochemical concentration[5] and reduction of CO_2[6] are required for renewable routes to C-based fuels and chemicals not derived from biomass. Our research has studied both of these aspects of CO_2 chemistry, and the electrochemical concentration of CO_2 from 0.5% CO_2 feed streams to nearly 100% CO_2 in the exit gas streams has been reported for a single

Chart 1. Late-Transition-Metal Phosphine Complexes Containing Weakly Bound Acetonitrile Ligands (L)

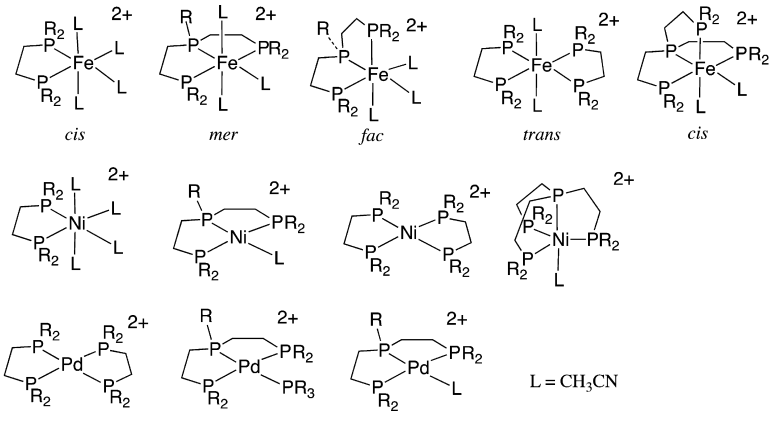

dx.doi.org/10.1021/ic4026969 | Inorg. Chem. 2014, 53, 3935−3960

pumping cycle.[7] In this perspective, only molecular electrocatalysis of CO_2 reduction is discussed. In the mid-1980s, we began a series of studies to develop electrocatalysts for CO_2 reduction using transition-metal complexes containing phosphine ligands.[8−10] At that time, there were several molecular catalysts for the electrochemical reduction of CO_2 to either CO or formate based on transition-metal complexes with either N-based macrocyclic ligands or bipyridine ligands.[11] There were also preliminary studies that indicated that phosphine-based complexes might also be active as electrocatalysts. For example, Darensbourg and co-workers had shown that *trans*-$[(H)_2Ni(PCy_3)_2]$ inserted CO_2 to form *trans*-$[(H)(HCO_2)Ni(PCy_3)_2]$,[12] and Slater and Wagenknecht demonstrated the stoichiometric electrochemical reduction of CO_2 to formate using a $[Rh(diphosphine)_2]^+$ complex.[13]

Our efforts focused on late-transition-metal complexes of the Fe, Co, and Ni triads that would not form the strong M−O bonds associated with early transition metals. We also wanted to examine how the number of weakly coordinating ligands would affect CO_2 binding, activation, and catalysis. To achieve these goals, a series of complexes containing bidentate, tridentate, and tetradentate phosphine ligands with acetonitrile ligands were synthesized and screened for electrocatalytic CO_2 reduction (Chart1; L = CH_3CN).[8] Our results indicated that some of the Fe complexes reacted with CO_2 when reduced, but this occurred at very negative potentials.[9] Although the Ni complexes studied were not catalysts for CO_2 reduction, they exhibited two closely spaced, one-electron reductions at potentials near those desired for the reduction of CO_2 to CO or formate. This led us to study Pd complexes as well, and it was found that $[Pd(triphosphine)(CH_3CN)]^{2+}$ complexes, the last entry in Chart 1, are active catalysts for CO_2 reduction to CO.[9,14]

Mechanistic studies of these Pd complexes suggested the catalytic cycle shown in Scheme 1.[14] At low acid concentrations, the catalytic rate exhibits a second-order dependence on the acid concentration, consistent with protonation of the bound CO_2 ligand, as shown in steps 3 and 6. Catalysis is inhibited by the presence of a strongly coordinating ligand such as dimethyl sulfoxide or a monodentate phosphine ligand. This inhibition was attributed to the requirement for a vacant coordination site for cleavage of the C−O bond, as shown in step 7. At acid concentrations above 0.02 M, the rate-determining reaction in the catalytic cycle is step 2, which involves a nucleophilic attack of a Pd^I species on CO_2. This conclusion is supported by the observation that a plot of log(k) versus the potential of the $Pd^{II/I}$ couple is linear when the substituents on the central P atom are small, e.g., when R is a methyl or phenyl group (black diamonds in Figure 3).[15]

Scheme 1. Mechanism of CO_2 Reduction by $[Pd(triphosphine)(solvent)]^{2+}$ Complexes (L = Triphosphine Ligand; solvent = Acetonitrile or DMF)

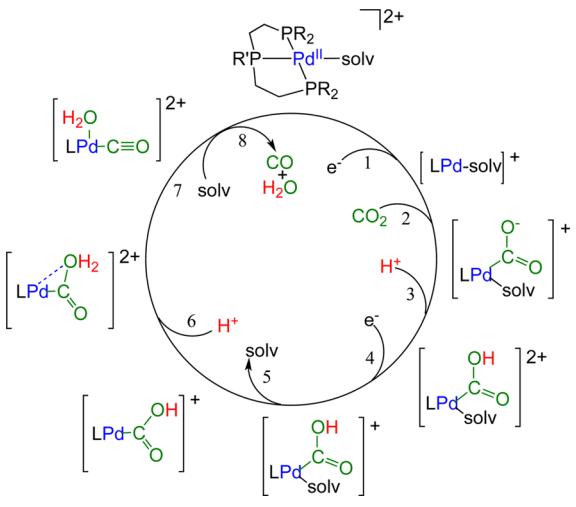

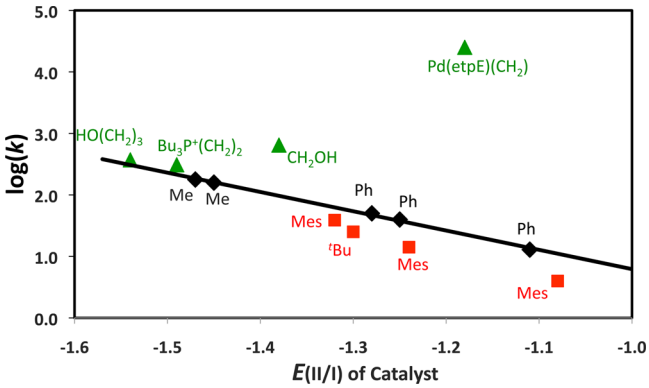

Figure 3. Plot of the log of the second-order rate constants for the reaction of $[Pd(triphosphine)(solvent)]^+$ with CO_2 (k) versus the $Pd^{II/I}$ potentials. The black diamonds are for complexes with small substituents (Me or Ph) on the central P atom of the tridentate ligand. The red squares represent complexes with large substituents on the central P atom. The green diamonds represent complexes with substituents on the central P atom that can potentially stabilize the Pd^I CO_2 adduct by interaction with the negative charge on the O atoms of the metallocarboxylic acid intermediates.

Further attempts to optimize the first coordination sphere of this class of catalyst involved replacement of the central atom of the triphosphine ligand with N, O, As, and C donor atoms, all of which decreased the overall catalytic performance.[16] It is also possible to vary the size of the two rings formed upon coordination of the triphosphine ligand to Pd.[17] The most active catalysts are observed for triphosphine ligands with ethylene backbones that form two five-membered rings upon coordination to the metal. Complexes with two six-membered rings or one five-membered and one six-membered rings are less active than those with two five-membered rings. Thus, the optimal features of the first coordination sphere included a Pd atom bound to a triphosphine ligand with ethylene backbones and a weakly coordinating solvent molecule such as acetontrile or dimethylformamide (DMF).

The performance characteristics of these $[Pd(triphosphine)(solvent)]^{2+}$ complexes in DMF solutions are indicated by their rates, selectivities, overpotentials (OPs), and turnover numbers (TONs). These complexes exhibit second-order rate constants as high as 300 M^{-1} s^{-1},[18] selectivities approaching 100% for CO production,[15] OPs ranging from 0.1 to 0.6 V,[15,16] and TONs greater than 2000.[19] A somewhat typical complex is $[Pd(PhP(CH_2CH_2PCy_2)_2)(CH_3CN)](BF_4)_2$, which catalyzes the reduction of CO_2 (at 1.0 atm of CO_2) to CO in acidic (>0.02 M HBF_4) DMF solutions containing 0.2 M NEt_4BF_4 with a turnover frequency (TOF) of 10 s^{-1}, a current efficiency (CE, a measure of selectivity) of 99%, a TON greater than 130, and an OP of approximately 0.3 V (−1.28 V vs the ferrocenium/ferrocene couple at a pH of 2).[14,15] The experimental conditions used in these studies were not optimized in terms of their rates, TONs, CEs, or OPs; rather a common set of

dx.doi.org/10.1021/ic4026969 | Inorg. Chem. 2014, 53, 3935−3960

experimental conditions were used for determining the structure–activity relationships.

Studies on the Role of the Second Coordination Sphere of Molecular Electrocatalysts for CO_2 Reduction. As discussed above, the rate-determining step under normal operating conditions (excess acid and 1.0 atm of CO_2) is the reaction of a Pd^I intermediate with CO_2, as shown in step 2 of Scheme 1. For small substituents on the central P atom of the tridentate ligand, the log of this second-order rate constant increases linearly with the potential of the $Pd^{II/I}$ couple, as shown by the black diamonds in Figure 3.[14] However, when the substituent on the central P atom is large, for example when R′ is a mesityl or *tert*-butyl substituent, the observed catalytic rate decreases by a factor of approximately 2, as shown by the red squares in Figure 3.[15] This is consistent with a large substituent preventing the coordination of CO_2 to the face of the catalyst adjacent to R′, as shown in structure **3**, but not to the face opposite R′, structure **4**. In this case, the second coordination sphere is inhibiting catalysis.

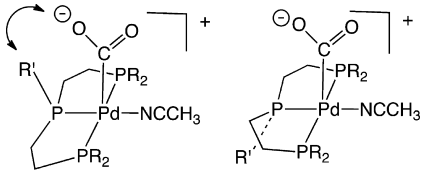

3 **4**

However, if the substituents R′ were designed to facilitate CO_2 binding to the Pd^I center, it might be possible to accelerate the overall rate of catalysis. One approach to achieving this objective was to attach positively charged phosphonium substituents via an ethylene linker to the central P atom of the triphosphine ligand, as shown in structure **5**.[20] In this case, the observed catalytic rates increased slightly, approximately 50%. Similarly, a 3-hydroxypropyl substituent was introduced, as shown in structure **6**, to explore whether hydrogen bonding between the proton on the hydroxyl group and the O atom of the bound CO_2 would facilitate CO_2 binding.[18] However, as can be seen from Figure 3, no rate enhancement was observed. Finally, a second [Pd(triphosphine)(solvent)]$^{2+}$ unit was attached to the central P atom via a methylene link, as shown by structure **7** of Scheme 2.[21] For this bimetallic complex, the second-order catalytic rate constant is greater than 2.5×10^4 M^{-1} s^{-1}, which corresponds to an enhancement of over 3 orders of magnitude from that expected for the $Pd^{II/I}$ reduction potential observed, as shown in Figure 3. Although the TOF for this complex is high, the TON is extremely low, approximately 10. This low TON is attributed to the rapid formation of a Pd–Pd bond. This same process leads to deactivation of the mononuclear [Pd(triphosphine)(solvent)]$^{2+}$ analogues with small terminal substituents.[14] The high catalytic rate of complex **7** suggests that similar complexes that do not form metal–metal bonds would be of interest. This could possibly be achieved by the use of first-row transition metals, which form weaker M–M bonds, or heterobimetallic complexes with metal centers that reduce at significantly different potentials.

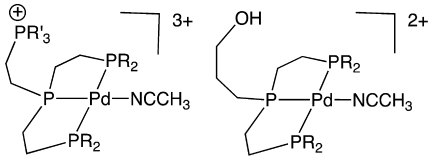

5 **6**

The [NiFe]-CO dehydrogenase enzyme ([NiFe]-CODH) is another catalyst that is highly active for the reduction of CO_2 to CO.[22] This catalyst is capable of reversibly catalyzing the oxidation of CO to CO_2 with a TOF of 3×10^4 s^{-1}, and it has been characterized by a number of recent X-ray diffraction studies.[23,24] Of particular interest is a study by Dobbek and co-workers in which they report the structures of the active site in the oxidized form and the reduced form in the presence of CO_2.[23] Structures **8** and **10** of Scheme 2 illustrate some of the important features of this active site. The active site of the oxidized form of CO dehydrogenase, structure **8**, consists of a square-planar Ni center bound to three soft S ligands and a weakly bound bridging hydroxide or water molecule. In comparison, the isoelectronic square-planar Pd centers of the bimetallic complex coordinate three soft P atoms and a weakly bound solvent molecule. The presence of a weakly bound fourth ligand in the oxidized forms of both the [NiFe]-CO dehydrogenase active site, **8**, and the synthetic catalyst, **7**, suggests that this is also an important feature for highly active CO_2 reduction catalysts.

Scheme 2. Comparison of the Structures of [NiFe]-CODH and a Bimetallic Pd Catalyst

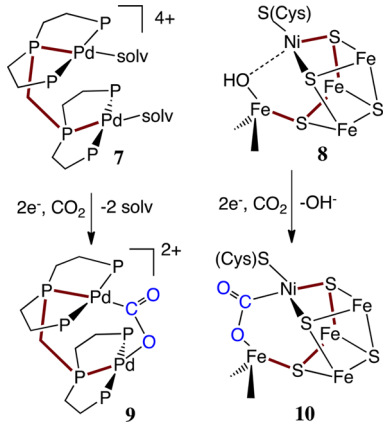

In structures **8** and **10**, the Ni center is connected via a three-atom sequence, S–Fe–S highlighted with red bonds, to a terminal Fe center. For the bimetallic Pd complexes, **7** and **9**, the two Pd centers are connected via a three-atom P–C–P sequence, also highlighted with red bonds. Reduction of the [NiFe]-CO dehydrogenase active site in the presence of CO_2 leads to the bifunctional activation of CO_2 in which the Ni center binds to the C atom of CO_2 and the Fe center binds to a negatively charged O atom of reduced CO_2, structure **10**.[23] This binding mode is nearly identical with that proposed approximately 10 years earlier for the reduced form of the bimetallic Pd complex **9**.[16] The similarities of structures **9** and **10** suggest that the basic structural motif of a three-atom chain connecting two metal centers meets the minimal requirements for the rapid binding and activation of CO_2. Studies in our laboratories in which the methylene group in structure **7** was replaced with a benzene ring with the central P atoms attached

dx.doi.org/10.1021/ic4026969 | Inorg. Chem. 2014, 53, 3935–3960

in meta positions, **11**, resulted in a catalyst for which there is no evidence for bifunctional CO_2 activation and with a catalytic rate very similar to that reported for the mononuclear analogue.[19] Similarly, dendrimers, in which [Pd(triphosphine)(solvent)]$^{2+}$ units are attached via ethylene linkers, as shown in structure **12**, have rates comparable to those of their simple mononuclear analogues.[25] Thus, the catalytic enhancement observed for the bimetallic complex **7** appears to be highly sensitive to the structure of the linker and the relative positioning of the two Pd centers. The rigidity of the three-atom linkage is likely much greater for structures **8** and **10** compared to **7** and **9** and suggests that a more rigid linker between the two metal centers in structures **7** and **9** may be beneficial. The high catalytic activities observed for **7** and **8** also suggest that the failure to observe significant rate enhancements for complexes **5** and **6** may result from the incorrect positioning of the positive charge in **5** and the hydroxyl group in **6**.

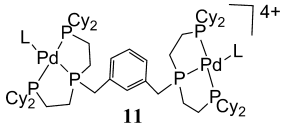

11

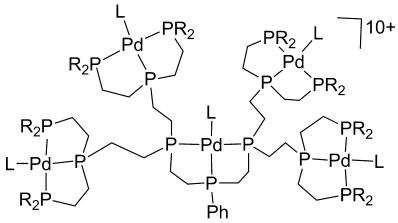

12

L = CH_3CN

The evolution of the Pd catalysts described above for electrocatalytic reduction of CO_2 to CO is an example of a modular approach to catalyst design.[26] The monometallic [Pd(triphosphine)(solvent)]$^{2+}$ complex described above with weakly bound solvent molecules, three P atoms in the tridentate ligand, and ethylene linkages between the P atoms is an example of first-coordination-sphere optimization. The investigation of different substituents on the triphosphine ligands and their role in facilitating or retarding CO_2 binding to the Pd^I complexes reflects efforts to understand the role of the second coordination sphere. Properly designed substituents can facilitate bifunctional CO_2 binding via a Pd–C bond and a second interaction with an O atom through hydrogen bonding, electrostatic interactions, or binding to a second metal. An important conclusion from these studies is that precise control of the positioning of the functional group in the second coordination sphere appears to be required. In structures **8** and **10**, this control is achieved by the incorporation of a rigid three-atom linker that determines the distance between the two metal centers. In the bimetallic complex **7**, large rate enhancements are observed as a result of bifunctional activation via a rotationally flexible P–C–P linker between the two Pd centers. It will be of interest to see if more rigid linkers than the P–C–P motif will produce even greater rate enhancements for synthetic catalysts. Although the [Pd(triphosphine)(solvent)]$^{2+}$ catalysts and their bimetallic analogues are not fully optimized, they illustrate the use of a modular approach for the development of a new class of electrocatalysts for the reduction of CO_2 to CO.

■ ENERGY-BASED APPROACH TO CATALYSIS

Thermodynamic Studies of Hydride-Transfer Reactions. Our interest in developing an energy-based or thermodynamic approach to catalysis arose from the fact that the CO produced by electrocatalytic reduction of CO_2 by the catalysts discussed in the preceding section is not an ideal fuel. As a result, we began to explore the possibility of developing molecular electrocatalysts for the reduction of CO. Although nitrogenase enzymes can reduce CO,[27] there are no known synthetic electrocatalysts for CO reduction. Borohydride reagents have been reported to reduce rhenium carbonyl complexes to formyl, hydroxymethyl, and methyl complexes.[28] Our research sought to replace the borohydride reagents with transition-metal hydrides that could be generated either electrochemically or from direct reaction with H_2 gas. In 1993, we reported that [$HNi(dmpe)_2$](PF_6) and [$HPt(depe)_2$](PF_6) could be generated by electrochemical reduction of [$Ni(dmpe)_2$](PF_6)$_2$ and [$Pt(depe)_2$](PF_6)$_2$ in protic media [where dmpe is bis(dimethylphosphino)ethane and depe is bis(diethylphosphino)ethane].[29] These complexes could also transfer their hydride ligands to a variety of cationic metal carbonyl complexes to form formyl complexes in stoichiometric reactions, as shown in reaction (1) for [$HNi(dmpe)_2$]$^+$ (**13**) and [$CpRe(NO)(CO)_2$]$^+$ (**14**).

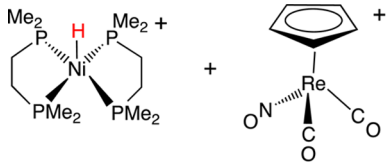

13 **14**

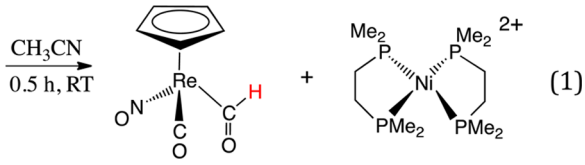

15 **16** (1)

Reaction (1) involves a formal transfer of a hydride ligand from a transition metal to a C atom of a coordinated CO ligand. The ability to predict whether such a hydride-transfer reaction should occur requires information on the relative hydride donor abilities of transition-metal hydrides such as **13** and transition-metal formyl complexes such as **15**. At that time, there had been a number of studies describing the *kinetic* hydride donor abilities (or hydricities) of transition-metal complexes,[30] but there were no thermodynamic studies of this property. However, knowledge of the hydride donor abilities is key to understanding a wide range of stoichiometric and catalytic reactions. To address this issue, we applied the thermodynamic cycle shown in Scheme 3 (reactions 2–5, where M = Ni, Pd, and Pt and L = diphosphine ligand) to determine the hydride donor/acceptor abilities of [HM(diphosphine)$_2$]$^+$ complexes.[31] Parker and co-workers had used this cycle previously to determine the hydride donor abilities of organic compounds such as hydroquinone anions.[32] As shown in reaction 2, the pK_a values for the [HM(diphosphine)$_2$]$^+$ complexes can be determined from equilibrium measurements using bases whose pK_a values are known in acetonitrile. In addition, [M(diphosphine)$_2$]$^{2+}$ complexes (where M = Ni, Pd, and Pt) undergo two reversible one-electron

dx.doi.org/10.1021/ic4026969 | Inorg. Chem. 2014, 53, 3935–3960

reductions or a single reversible two-electron reduction, as shown in reaction 3. To complete the cycle, the potential of the H^+/H^- couple versus the ferrocenium/ferrocene couple in acetonitrile is needed (reaction 4), and this constant (79.6 kcal/mol) rests on extrathermodynamic assumptions, as discussed elsewhere.[33] The sum of reactions 2−4 is the heterolytic cleavage of the M−H bond to form the corresponding metal fragment and H^- (reaction 5), and the free energy associated with this reaction is simply the sum of the free energies associated with reactions 2−4, $\Delta G^\circ_{H^-}$. Using this approach, we reported the first *thermodynamic* measurements of transition-metal hydride donor abilities, or hydricities, in 1999 with $\Delta G^\circ_{H^-}$ values varying by 21 kcal/mol depending on the metal, ligand substituents, and size of the chelate bite of the diphosphine ligand.[31] $[HPt(dmpe)_2]^+$ with a $\Delta G^\circ_{H^-}$ value of 42.0 kcal/mol is a 21 kcal/mol better hydride donor than $[HNi(dppe)_2]^+$ [where dppe is 1,2-bis(diphenylphosphino)-ethane] with a value of 62.8 kcal/mol. A smaller value of $\Delta G^\circ_{H^-}$ corresponds to a better hydride donor, while a larger $\Delta G^\circ_{H^-}$ value corresponds to a greater hydride acceptor ability of the corresponding $[M(diphosphine)_2]^{2+}$ complex.

The ability to measure the hydride donor abilities for transition-metal hydrides immediately raised a number of interesting questions. For example, are there other methods of measuring hydride donor/acceptor abilities in addition to the thermodynamic cycle shown in Scheme 3 that would provide confidence regarding the internal consistency of these new hydride donor/acceptor values and extend the range of compounds that can be studied? Can hydride donor/acceptor values be measured for a number of other classes of compounds to provide a more general picture of hydride donor/acceptor abilities? For the $[HM(diphosphine)_2]^+/[[M(diphosphine)_2]^{2+}$ complexes, what are the factors that control their hydride donor/acceptor abilities? Can more complex and complete thermodynamic descriptions be developed for transition-metal dihydrides and trihydrides? What are the relationships between different thermodynamic properties? Can predictive models be developed? What does this information tell us about chemical reactivity and catalysis? Our attempts to answer these questions resulted in a significant shift in the focus of our research efforts.

Methods of Measuring the Hydride Donor/Acceptor Abilities Referenced to pK_a Scales. Scheme 3 illustrates a thermodynamic cycle for determining hydride donor/acceptor abilities based on measurements of pK_a values and redox potentials. A second method for determining hydride donor abilities is shown in Scheme 4. This thermodynamic cycle is based on the reversible heterolytic formation/cleavage of H_2. Examination of eqs 2 and 7 of Schemes 3 and 4 indicates that both of these methods rely on pK_a values of protonated bases. Fortunately, considerable effort has recently been devoted to developing internally consistent pK_a scales for a large range of protonated bases in acetonitrile.[34] Although the two cycles shown in Schemes 3 and 4 require known pK_a values of reference compounds, they do not require the hydride donor abilities of reference compounds. In this regard, they are absolute methods that tie the hydride donor abilities to pK_a scales. However, these two thermodynamic cycles require free-energy values for the two-electron-reduction potential of a proton to a hydride (eq 4) or for heterolytic cleavage of H_2 to form a solvated proton and hydride (eq 8). Determining these values requires the use of extrathermodynamic assumptions, and this can lead to errors in these values.[33] The hydride donor abilities obtained using the methods shown in Schemes 3 and 4 agree within 1 kcal/mol.[35] This observed agreement is well within the estimated experimental error using either method, ±2 kcal/mol.[31,35] Thus, the constants used in eqs 4 and 8 have sufficient internal consistency to allow the hydride donor abilities obtained using Scheme 3 to predict protonated bases

Scheme 3. Electrochemical Method for Determining Hydride Donor Abilities

	ΔG° (kcal/mol)	
$[HML_2]^+ \rightarrow ML_2 + H^+$	$1.37pK_{a(MH)}$	(2)
$ML_2 \leftrightarrows [ML_2]^{2+} + 2\,e^-$	$46.1E^\circ(II/0)$	(3)
$H^+ + 2\,e^- \rightarrow H^-$	$-46.1E^\circ(H^+/H^-)$ (79.6 kcal/mol)	(4)
$[HML_2]^+ \rightarrow [ML_2]^{2+} + H^-$	$\Delta G^\circ_{H^-} = 1.37pK_{a(MH)} + 46.1E^\circ(II/0) + 79.6$	(5)

Scheme 4. Determining Hydride Donor Abilities by Heterolytic Cleavage of H_2

	ΔG° (kcal/mol)	
$[HML_2]^+ + BaseH^+ \leftrightarrows [ML_2]^{2+} + H_2(g) + Base$	$-1.37\log(K_{eq})$	(6)
$Base + H^+ \rightarrow BaseH^+$	$-1.37pK_{(BH^+)}$	(7)
$H_{2(g)} \rightarrow H^+ + H^-$	76.0 kcal/mol	(8)
$[HML_2]^+ \rightarrow [ML_2]^{2+} + H^-$	$\Delta G^\circ_{H^-} = -1.37\log(K_{eq5}) - 1.37pK_{(BH^+)} + 76.0$	(9)

dx.doi.org/10.1021/ic4026969 | *Inorg. Chem.* 2014, 53, 3935−3960

(acids) with appropriate pK_a values for observing equilibria for reaction (6), the heterolytic cleavage/formation of H_2.

Relative Methods. The most intuitive and simplest method for determining the hydride donor abilities relies on equilibrium measurements of hydride-transfer reactions between hydride donors, L_nMH, and hydride acceptors, A, as shown in Scheme 5, reaction (10). If an equilibrium is observed, eq 11 can be used to calculate $\Delta G^\circ_{H^-}$. This method requires a value for the equilibrium constant for reaction (10) and the hydride donor ability of the reference compound, AH^-.

Scheme 5. Determining Hydride Donor Abilities by Hydride-Transfer Reactions

$$L_nMH + A \leftrightarrows L_nM^+ + AH^- \quad (10)$$

$$\Delta G^\circ_H\text{-}(L_nMH) = \Delta G^\circ_H\text{-}(AH^-) + \Delta G^\circ_{10} \quad (11)$$

Reactions (12)−(14) show *reversible* hydride-transfer reactions that have been used to establish the relative hydricity of metal hydrides, formyl complexes, and NADH model compounds, such as 1-benzyl-1,4-dihydronicotinamide.[36,37] The use of eq 11 requires a reference compound. In reaction (12), the reference compound is $[HPt(dmpe)_2]^+$, whose hydride donor ability was determined as shown in Schemes 3 and 4 to establish an absolute scale, i.e., one referenced to a pK_a scale. In this way, the hydride-transfer reactions (12)−(14) can be placed on the pK_a-referenced scale. Direct hydride-transfer reactions have also been used to establish the hydride donor abilities of borohydride compounds.[38,39] A practical consideration for direct hydride-transfer reactions is their rates. Hydride transfer between two metal centers frequently requires several days to weeks, presumably because of the charge and steric repulsions involved in the close approach of two metal centers.[36,37] However, the formyl complexes shown in reactions (12)−(14) are neutral, and the hydride ligand is located on the exterior of the molecule so that large reorganization energies are not required for the close approach that occurs during hydride transfer. As a result, hydride transfers from formyl complexes, such as those shown in reactions (13) and (14), are much faster (reaching equilibrium in minutes to hours) than those from metal hydrides.

$$[HPt(dmpe)_2]^+ + [CpRe(PMe_3)(NO)(CO)]^+ \leftrightarrows [Pt(dmpe)_2]^{2+} + CpRe(PMe_3)(NO)(CHO) \quad (12)$$

$$CpRe(PMe_3)(NO)(CHO) + [CpRe(PPh_3)(NO)(CO)]^+ \leftrightarrows [CpRe(PMe_3)(NO)(CO)]^+ + CpRe(PPh_3)(NO)(CHO) \quad (13)$$

$$\text{benzyl-NADH} + [CpRe(NO)(CO)_2]^+ \leftrightarrows \text{benzyl-NAD}^+ + CpRe(NO)(CO)(CHO) \quad (14)$$

Another method for determining the relative hydride donor abilities involves ligand-exchange reactions. An example of this approach is shown in Scheme 6, reactions (15)−(18), which were studied by $^{31}P\{^1H\}$ NMR spectroscopy.[38] The free energy of the hydride ligand exchange as shown in eq 19 is the sum of the hydride donor ability of the reference compound, in this case $HRh(depe)_2$, and the free energies associated with ligand exchange for the hydride complexes and corresponding hydride acceptor complexes. These four methods, two absolute and two relative, illustrate different experimental approaches that can be used to determine the hydride donor abilities.

Overview of the Hydride Donor Abilities of Different Classes of Compounds. The different methods described in the preceding section provide a versatile set of tools for determining the hydride donor abilities of a broad range of compounds, as shown in Figure 4. The total range spans over 100 kcal/mol. For convenience, we tend to classify hydride donors as compounds having $\Delta G^\circ_{H^-}$ values less than 76 kcal/mol (the hydride donor ability of H_2 gas in equilibrium with 1.0 M H^+ in acetonitrile) and hydride acceptors as those having hydride donor abilities greater than 76 kcal/mol (these compounds are shown in their hydride acceptor form in Figure 4). By these criteria, triarylcarbonium ions,[40] quinones,[32] and the manganese oxo complex[41] are good hydride acceptors (better than H^+), although the carbonium ions and quinones span large ranges. Analogues of NADH, the hydride donor used in biological systems, are moderate hydride donors.[37,42]

$\Delta G^\circ_{H^-}$ values for heterolytic cleavage of the C−H bonds of formyl complexes, NADH model compounds, and triarylmethane derivatives span a range of 72 kcal/mol, ranging from moderately good hydride donors to powerful hydride acceptors.[40] The formyl complexes of the general formula CpRe(NO)(L)(CHO) (where L = CO or PR_3) are the best hydride donors of this class:[36] better than NADH compounds[37,42] and much better than triarylmethane compounds.[40] $\Delta G^\circ_{H^-}$ values for heterolytic cleavage of the O−H bonds of hydroquinone anions and $[(phen)_2Mn^{III}(\mu\text{-}O)(\mu\text{-}OH)Mn^{III}(phen)_2]^{3+}$ span a large range from 70 to 122 kcal/mol.[32,41] A comparison of the hydride donor abilities of the H−O(Y) bonds of quinones and $[(phen)_2Mn^{III}(\mu\text{-}O)(\mu\text{-}OH)Mn^{III}(phen)_2]^{3+}$ with the H−S

Scheme 6. Determining Hydride Donor Abilities by Ligand-Exchange Reactions

$$HRh(depe)_2 \rightarrow [Rh(depe)_2]^+ + H^- \qquad \Delta G^\circ_H\text{-}(depe) \quad (15)$$

$$[Rh(depe)_2]^+ + 2dmpe \leftrightarrows [Rh(dmpe)_2]^+ + 2depe \qquad \Delta G^\circ_H\text{-}(ML_n^+/ ML'^+_n) \quad (16)$$

$$HRh(dmpe)_2 + 2depe \leftrightarrows HRh(depe)_2 + 2dmpe \qquad \Delta G^\circ_H\text{-}(HML_n/ HML'_n) \quad (17)$$

$$HRh(dmpe)_2 \rightarrow [Rh(dmpe)_2]^+ + H^- \quad (18)$$

$$\Delta G^\circ_H\text{-}(dmpe) = \Delta G^\circ_H\text{-}(depe) + \Delta G^\circ_H\text{-}(ML_n^+/ ML'^+_n) + \Delta G^\circ_H\text{-}(HML_n/ HML'_n) \quad (19)$$

dx.doi.org/10.1021/ic4026969 | Inorg. Chem. 2014, 53, 3935−3960

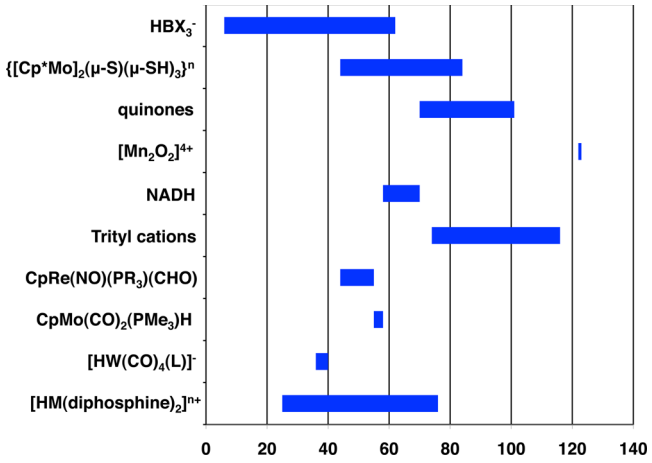

Figure 4. Hydride donor abilities ($\Delta G^\circ_{H^-}$) of various classes of compounds in acetonitrile. HBX_3^- represents a series of borohydride derivatives (refs 38 and 39); $\{Cp^*Mo]_2(\mu\text{-}S)(\mu\text{-}SH)_3\}^n$ represents a series of Mo complexes with bridging SH ligands (ref 43); $[Mn_2O_2]^{4+}$ represents the hydride acceptor form of $[(phen)_2Mn^{III}(\mu\text{-}O)(\mu\text{-}OH)Mn^{III}(phen)_2]^{3+}$ (phen = 1,10-phenanthroline; ref 41); NADH represents a series of 1-substituted 1,4-dihydronicotinamide derivatives (refs 37 and 42); quinones represent a series of hydroquinone anions whose corresponding hydride acceptors are quinones (ref 32); trityl cations represent a series of triarylmethane complexes whose corresponding hydride acceptors are trityl cations (ref 40); $CpRe(NO)(PR_3)(CHO)$ represents a series of rhenium formyl complexes (ref 36); $CpMo(CO)_2(PMe_3)H$, $[HW(CO)_4(L)]^-$, and $[HM(diphosphine)_2]^{n+}$ represent three different classes of transition-metal hydride complexes (refs 31, 35, 37, 38, and 44–53).

bonds of the bridging hydrosulfido ligands of $[Cp^*Mo(\mu\text{-}S)_x(\mu\text{-}SH)_{4-x}MoCp^*]^n$ complexes indicates that the hydride donor abilities of the latter complexes span a range of 44–84 kcal/mol,[43] somewhat overlapping the range of hydride donor abilities of hydroquinone anions. However, the SH group is a much better hydride donor than an OH group in a similar environment. From these comparisons, it can be seen that the hydride donor abilities of an H–X(Y) bond (where X represents the atom bound directly to H and Y signifies the remainder of the molecule) depend a great deal on the identitiy of both Y and X.

The range of hydride donor abilities (6–62 kcal/mol) shown in Figure 4 for $[HBX_3]^-$ compounds is based on density functional theory (DFT) calculations for isodesmic reactions between $[HBEt_3]^-$ and BX_3 to form $[HBX_3]^-$ and BEt_3.[39] One of these compounds, $[HBEt_3]^-$, has been experimentally cross-referenced to $HRh(dmpe)_2$ with a hydride donor ability of 26 kcal/mol.[38] These $[HBX_3]^-$ compounds are clearly better hydride donors than the various classes of organic compounds, and this is consistent with the utility of borohydrides as reducing agents in a large range of organic reactions. Similarly, the borohydride reagents are better hydride donors than the formyl complexes discussed above and the transition-metal hydride complexes discussed in the next paragraph. As a result, the borohydride reagents can be used to reduce metal carbonyl complexes to formyls and transition-metal complexes to form transition-metal hydrides. While these statements are true in a general sense, there are broad ranges of overlap. As will be discussed in more detail under applications, quantitative applications of hydricity scales can be used to determine when these general observations will and will not serve as useful guides.

Transition-metal hydrides are good hydride donors, with a range of 26–76 kcal/mol (Figure 4). They are generally better hydride donors than the organic compounds shown, although again there is considerable overlap, especially with the formyl complexes and NADH derivatives. As expected, the anionic hydrides of the formula $[HM(CO)_4L]^-$ [where M = Cr and W and L = CO, PR_3, and $P(OR)_3$] are better hydride donors than the neutral $CpMo(CO)_2(PMe_3)H$, $Cp^*Mo(CO)_2(PMe_3)H$, and $CpW(CO)_2(IMes)H$ complexes [IMes = 1,3-bis(2,4,6-trimethylphenyl)imidazol-2-ylidene].[37,44,45] The $[HM(CO)_4L]^-$ complexes are synthetically useful in the reduction of alkyl halides, aldehydes, ketones, and other substrates.[30c–f] Kinetic studies of $[HW(CO)_4P(OMe)_3]^-$ suggest that the nucleophilicity of this complex is comparable to that of lithium triethylborohydride. However, thermodynamic studies indicate that $[HW(CO)_4P(OMe)_3]^-$ is a poorer hydride donor than $[HBEt_3]^-$ by 11 kcal/mol.[38] This clearly demonstrates that nucleophilicity and thermodynamic hydride donor abilities (or hydricities) of transition-metal hydrides can be significantly different. The transition-metal hydrides that have been studied in most detail are those of the $[HM(diphosphine)_2]^+$ and $HM'(diphosphine)_2$ classes (M = Ni, Pd, and Pt and M′ = Co and Rh).[31,35,38,46–54] It is clear from Figure 4 that the hydride donor abilities of these compounds span a large range with hydride donor abilities comparable to those of $[HBEt_3]^-$ for the more hydridic complexes to those that overlap with triphenylaryl compounds.

Factors Controlling the Thermodynamic Properties of $[HM(diphosphine)_2]^+$ and $HM'(diphosphine)_2$ Complexes (M = Ni, Pd, and Pt and M′ = Co and Rh). Equation 20 shows the relationship between pK_a values, homolytic bond dissociation free energies ($\Delta G^\circ_{H^\bullet}$), and redox potentials of the $M^{I/0}$ or $M'^{0/1-}$ couples of the corresponding $[M(diphosphine)_2]^+$ and $M'(diphosphine)_2$ complexes derived from thermodynamic cycles for acetonitrile solutions. If the homolytic bond dissociation free energies of $[HM(diphosphine)_2]^+$ or $HM'(diphosphine)_2$ complexes are constant for a particular metal, then the pK_a values should show a linear relationship with the potential of the $M^{I/0}$ or $M'^{0/1-}$ couples, respectively, of the corresponding $[M(diphosphine)_2]^+$ and $M'(diphosphine)_2$ complexes. Both experimental and theoretical studies show that there is such a linear relationship, as shown in the top graph of Figure 5 for $[HNi(diphosphine)_2]^+$ complexes.[49,54–58] Small variations from the value of the slope shown in eq 20 are expected to arise from differences in the electronegativities of H and the metal center.

$$pK_a(M{-}H) = -16.8E_{1/2}(I/0) + 0.73(\Delta G^\circ_{H^\bullet} - 53.6) \quad (20)$$

Similarly, the free energy associated with heterolytic cleavage of an M–H bond ($\Delta G^\circ_{H^-}$) of $[HM(diphosphine)_2]^+$ or $HM'(diphosphine)_2$ complexes to form a solvated hydride ligand and the corresponding $[M(diphosphine)_2]^{2+}$ or $[M'(diphosphine)_2]^+$ complexes, respectively, is given by eq 21 for acetonitrile solutions. Because the homolytic bond dissociation energy ($\Delta G^\circ_{H^\bullet}$) is nearly constant for a given metal, $\Delta G^\circ_{H^-}$ also exhibits a linear correlation with the $M^{II/I}$ or $M'^{I/0}$ couples of the corresponding $[M(diphosphine)_2]^{2+}$ or $M'(diphosphine)_2]^+$ complexes, as shown by the bottom plot of Figure 5. The potentials of the $M^{II/I}$ or $M'^{I/0}$ couples for a given metal and the $\Delta G^\circ_{H^-}$ values are affected by two parameters. One parameter is the electron-withdrawing or -donating abilities of the substituents on the diphosphine ligands.[31,54]

dx.doi.org/10.1021/ic4026969 | Inorg. Chem. 2014, 53, 3935–3960

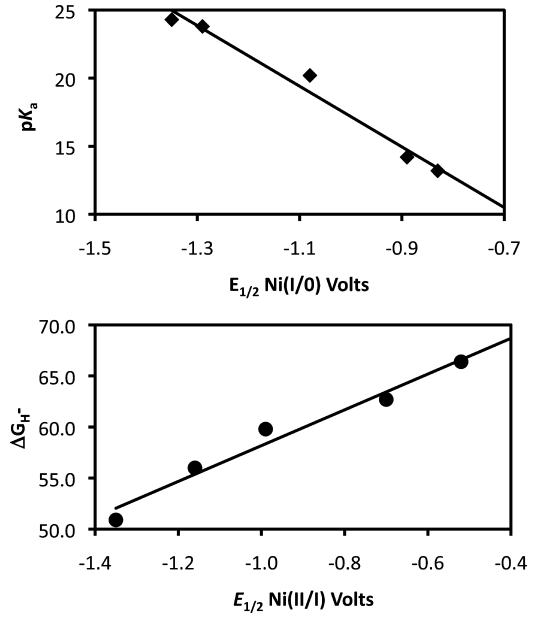

Figure 5. Plot of pK_a versus the half-wave potential of the $Ni^{I/0}$ couple in acetonitrile (top graph). Plot of $\Delta G^\circ_{H^-}$ versus the half-wave potential of the $Ni^{II/I}$ couple in acetonitrile (bottom graph). Potentials are referenced to the ferrocenium/ferrocene couple. Data were taken from ref 54.

As the substituents become more electron-rich, the hydride donor abilities of the $[HM(diphosphine)_2]^+$ and $HM'(diphosphine)_2$ complexes become greater ($\Delta G^\circ_{H^-}$ decreases).

$$\Delta G^\circ_{H^-} = 23.06E_{1/2}(II/I) + \Delta G^\circ_{H^\bullet} + 26.0 \quad (21)$$

The second parameter controlling the potentials of the $M^{II/I}$ or $M'^{I/0}$ couples of $[M(diphosphine)_2]^{2+}$ or $[M'(diphosphine)_2]^+$ complexes and the hydride donor ability of the corresponding $[HM(diphosphine)_2]^+$ or $HM'(diphosphine)_2$ complexes is the dihedral angle between the two planes defined by the P atoms of each of the diphosphine ligands and the metal center.[49,55,56] This dihedral angle is determined by interligand steric interactions between substituents on the two diphosphine ligands. As the dihedral angle between the two diphosphine ligands increases for ligands with bulkier substituents and/or larger ring sizes, the antibonding overlap between the P σ orbitals and the $d_{x^2-y^2}$ orbitals of the metal decreases, lowering the energy of the lowest unoccupied molecular orbital (LUMO). As a result, the $[M(diphosphine)_2]^{2+}$ or $[M'(diphosphine)_2]^+$ complexes become easier to reduce and better hydride acceptors, while the corresponding $[HM(diphosphine)_2]^+$ or $HM'(diphosphine)_2$ complexes become poorer hydride donors. This steric interaction can be used to control the potential of the $M^{II/I}$ or $M'^{I/0}$ couples without changing the potentials of the $M^{I/0}$ or $M'^{0/1-}$ couples.[31,56] Thus, the dihedral angle between the two diphosphine ligands provides a method for tuning the hydride donor abilities of these complexes independently from their pK_a values. This understanding of the factors controlling the acidity and hydride donor abilities of these complexes is useful in the design of both stoichiometric and catalytic reactions, as discussed in more detail below.

Finally, the identity of the metal also has a significant influence on the thermodynamic properties of $[HM(diphosphine)_2]^+$ and $HM'(diphosphine)_2$ complexes. For $[HM(diphosphine)_2]^+$ complexes (M = Ni, Pd, and Pt), the pK_a values of the nickel and platinum hydrides differ by approximately 6.5 ± 1.0 pK_a units for any given ligand, while palladium and nickel hydrides have nearly identical pK_a values.[31,48] For $\Delta G^\circ_{H^-}$, Pt complexes are better hydride donors than the corresponding Ni complexes by approximately 10 kcal/mol, and palladium hydride complexes are slightly better hydride donors than the corresponding platinum hydride complexes by approximately 3 kcal/mol. It is an interesting observation that the palladium hydride complexes are both better hydride donors and stronger acids than their Ni and Pt analogues. This has two consequences. First, the ability of a second-row metal hydride complex to be both a better hydride and proton donor than its first- or third-row analogues may contribute to the enhanced activity in catalytic reactions that is frequently observed for second-row transition metals. Second, the dependence of the hydride donor abilities and the acidities on the metal indicates that hydride donor abilities and acidities are independent properties; i.e., the acidities and hydride donor abilities of transition-metal hydrides are not necessarily inversely related to each other. The only thermodynamic property of the M−H bond to follow a periodic trend for the $[HM(diphosphine)_2]^+$ complexes is the homolytic bond dissociation free energy, which follows the order Pt−H (~68 kcal/mol) > Pd−H (~57 kcal/mol) > Ni−H (~54 kcal/mol).[48]

More Complete Thermodynamic Descriptions of Transition-Metal Hydrides, Dihydrides, and Trihydrides. Our initial thermodynamic studies focused on the hydride donor abilities of transition-metal hydride complexes because this previously unmeasured thermodynamic property was important for progress in developing complexes for CO reduction. However, combining hydride donor abilities with other known thermodynamic properties such as redox potentials, pK_a values, and homolytic bond dissociation free energies produces a more complete description of the transition-metal hydride bond and of the potential reactivity of this class of compounds.[46,51] An example is the thermodynamic diagram on the left side of Figure 6 for $[HNi(depp)_2]^+$ [where depp is 1,3-bis(diethylphosphino)-propane] showing the three modes of Ni−H bond cleavage (heterolytic with H^- formation, green arrow; homolytic with $H^\bullet$ formation, black arrow; heterolytic with H^+ formation, red arrow) and the two potentials for the electron-transfer reactions (blue arrows) that interconvert the corresponding Ni^{2+}, Ni^+, and Ni^0 species resulting from Ni−H bond cleavage.[31] If the values of the thermodynamic properties of any two sides of a triangle are known, then the value corresponding to the property indicated by the third side of the triangle can be calculated using a thermodynamic cycle.

From the thermodynamic diagram on the left side of Figure 6, it can be seen that hydride transfer (green arrow) can be regarded as equivalent to proton transfer (red arrow) and two electron-transfer reactions (blue arrows). Similarly, a homolytic bond cleavage can be regarded as equivalent to hydride and electron transfer (Ni^{2+}/Ni^+) or proton and electron transfer ($Ni^{+/0}$). If the electron and proton are transferred to another atom, this results in a net H-atom transfer between two atoms that may occur in a stepwise process (proton transfer followed by electron transfer, PTET, or electron transfer followed by proton transfer, ETPT) or a concerted process (EPT). In an electrochemical reaction, the electron can be reversibly transferred to an electrode and the proton transferred to a

dx.doi.org/10.1021/ic4026969 | Inorg. Chem. 2014, 53, 3935−3960

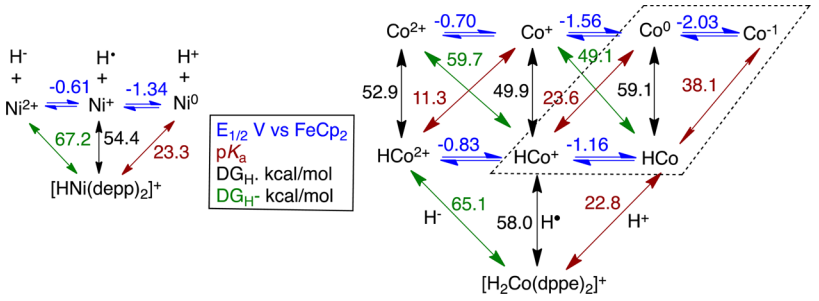

Figure 6. Thermodynamic diagrams for $[HNi(depp)_2]^+$ (left) and $[H_2Co(dppe)_2]^+$ (right) showing the relationships between the different thermodynamic properties for monohydride and dihydride species, respectively. All data are for acetonitrile solutions.

base in solution. In either case, the thermodynamics are the same.

The generalization of this approach to dihydrides is shown by the thermodynamic diagram on the right side of Figure 6 for $[H_2Co(dppe)_2]^+$.[46] The three bond cleavage reactions are again shown for the dihydride complex at the bottom of the diagram to form three monohydride species that can undergo the three different bond cleavage reactions whose species are related by electron-transfer reactions, as shown in blue. These different thermodynamic values determine the energetic relationships between all of the species shown. Even more complex diagrams have been obtained for trihydrides.[43] The significance of the data contained in the dashed parallelogram will be discussed in more detail below.

Correlations between Thermodynamic Properties. As shown by the linear plots in Figure 5, the potentials of the $Ni^{II/I}$ couples can be used to predict the hydride donor ability of $[HNi(diphosphine)_2]^+$ complexes and the potentials of the $Ni^{I/0}$ couples can be used to predict the pK_a values of these complexes.[49,54] DFT calculations carried out on a series of Ni, Pd, Pt, Co, and Rh complexes support the linear relationships observed experimentally.[55−58] In addition to the correlations between the redox potentials and the pK_a values and hydride donor abilities of these monohydrides, results from studies of a limited set of dihydride species ($[H_2Co(dppe)_2]^+$,[46] $[H_2Rh(depx)_2]^+$,[51] and $[H_2Pt(EtXantphos)_2]^{2+}$)[50] suggested linear relationships between the $M^{II/I}$, $M^{I/0}$, $M'^{I/0}$, and $M'^{0/1-}$ couples and other thermodynamic properties. An extensive set of calculations were carried out to confirm and extend these correlations for nickel bis(diphosphine) complexes.[55] Thermodynamic values calculated using a DFT-based isodesmic methodology were benchmarked against experimentally observed values and found to be accurate to within 2 kcal/mol. The theoretical methods developed were then extended to provide extensive data sets of calculated values, and these were used to construct correlations. The equations shown on the right side of Figure 7 relate the $Ni^{II/I}$ and $Ni^{I/0}$ couples to the set of thermodynamic parameters shown on the left side of Figure 7. Because the $Ni^{II/I}$ and $Ni^{I/0}$ couples can be measured by easily performed cyclic voltammetry experiments, these relationships provide a powerful tool for constructing thermodynamic schemes without the time-consuming efforts required to measure pK_a values or hydride donor abilities.

It can be seen from the equations of Figure 7 that pK_a(II), pK_a(III), and pK_a(IV) all depend on the potential of the $Ni^{I/0}$ couple with very similar slopes but significantly different intercepts. The pK_a(III) and pK_a(IV) values are much more negative than the value for pK_a(II) as a result of an increase in their positive charge. The values for the homolytic bond

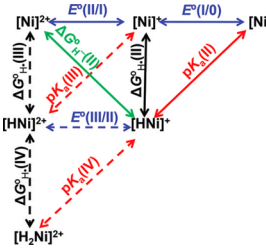

$pK_a(II) = -18.01E°(I/0) - 0.89$	(pK_a units)
$\Delta G°_{H^-}(II) = 21.72E°(II/I)) + 79.27$	(kcal/mol)
$E°(III/II) = 1.02E°(I/0) + 1.60$	(V)
$pK_a(III) = -18.38E°(I/0) - 27.82$	(pK_a units)
$pK_a(IV) = -16.90E°(I/0) - 24.78$	(pK_a units)
$\Delta G°H^•(II) = -1.34E°(II/I)) + 53.27$	(kcal/mol)
$\Delta G°H^•(III) = -25.05E°(I/0) +$ 23.06E°(II/I) + 15.65	(kcal/mol)
$\Delta G°H^•(IV) = 0.47E°(I/0) + 56.7$	(kcal/mol)

Figure 7. (Left) Thermodynamic diagram illustrating the thermodynamic parameters that relate the various Ni species to each other, where $[\mathbf{Ni}]^{2+}$ = $[Ni(diphosphine)_2]^{2+}$, $[\mathbf{Ni}]^{+}$ = $[Ni(diphosphine)_2]^{+}$, $[\mathbf{Ni}]^{0}$ = $Ni(diphosphine)_2$, $[\mathbf{HNi}]^{2+}$ = $[HNi^{III}(diphosphine)_2]^{2+}$, $[\mathbf{HNi}]^{+}$ = $[HNi(diphosphine)_2]^{+}$, and $[\mathbf{H_2Ni}]^{2+}$ = $[H_2Ni(diphosphine)_2]^{2+}$. (Right) Equations taken from ref 55 illustrating that all of the parameters shown on the left side can be calculated from the $Ni^{II/I}$ and $Ni^{I/0}$ couples.

dissociation free energies, $\Delta G°_{H^•}(II)$ and $\Delta G°_{H^•}(IV)$, have similar intercepts and a small dependence on the potentials of the $Ni^{II/I}$ and $Ni^{I/0}$ couples, respectively. For most complexes, these two homolytic bond dissociation energies will be similar [$\Delta G°_{H^•}(II) \sim 55$ kcal/mol and $\Delta G°_{H^•}(IV) \sim 57$ kcal/mol] and nearly constant. However, $\Delta G°_{H^•}(III)$ depends strongly but in opposite directions on the $Ni^{II/I}$ and $Ni^{I/0}$ couples. As a result of the opposite signs and slopes of nearly equal magnitude, changes in the potentials resulting from differences in the electron donor abilities of the substituents will tend to cancel each other out, and $\Delta G°_{H^•}(III)$ will not be strongly dependent on inductive effects. However, as discussed above, the $Ni^{II/I}$ couple is strongly dependent on the dihedral angle between the two diphosphine ligands, which, in turn, depends on the chelate bite size and steric bulk of the substituents on P. As this dihedral angle increases, either as a result of an increase in the chelate bite angle or size of the phosphine substituents, the $Ni^{II/I}$ couple becomes more positive, and this will result in larger $\Delta G°_{H^•}(III)$ values as the dihedral angle increases. Because $\Delta G°_{H^•}(IV)$ is nearly constant, increases in the dihedral angle will favor the oxidative addition of H_2 to $[Ni]^{2+}$ to form a nickel(IV) dihydride. Extension of these concepts to other square-planar d^8 complexes suggests that oxidative addition reactions will be favored as the chelate bite size or steric bulk of the substituents increases, as has been observed experimentally.[46,50,51,53] Finally, the hydride donor ability, as determined by $\Delta G°_{H^-}(II)$, depends in a linear fashion on the potential of only the $Ni^{II/I}$ couple. Similarly, pK_a(II) values depend only on the potential of the $Ni^{I/0}$ couple. These equations again illustrate that hydride donor abilities and pK_a values are independent and not simply the inverse of each other.

dx.doi.org/10.1021/ic4026969 | Inorg. Chem. 2014, 53, 3935−3960

Applications of Thermodynamic Diagrams: Reactivity, Free-Energy Landscapes, and Reaction Profiles. In the preceding section, we discussed the relationships between the various thermodynamic properties shown in Figure 7 for $[Ni(diphosphine)_2]^{2+}$ systems and suggested that some of these relationships can be used to understand trends in oxidative addition/reductive elimination reactions. The dotted parallelogram of Figure 6 contains the thermodynamic parameters needed for understanding the thermodynamic constraints of proton-coupled electron-transfer (PCET) reactions. Similarly, the stability of $[HM(diphosphine)_2]^{+}$ complexes over a range of pH values can be understood in terms of their hydride donor abilities and pK_a values. The pK_a values of $[HM(diphosphine)_2]^{+}$ complexes determine the pH below which $M(diphosphine)_2$ complexes will protonate to form the corresponding hydride, and the hydride donor ability can be used as shown in Scheme 4 to determine the pH below which $[HM(diphosphine)_2]^{+}$ complexes will protonate and eliminate H_2. An interesting result of this analysis is that $[HM(diphosphine)_2]^{+}$ complexes with large chelate bite angles will be stable over a larger range of pH values than those with small chelate bite angles.[49]

Our original objective was to develop a better understanding of the hydride donor abilities of transition-metal hydride complexes so that hydride-transfer reactions to metal carbonyl complexes to form formyl complexes [e.g., reaction (1)] could be predicted from a thermodynamic perspective. As a result of these studies, we were able to predict and observe the stoichiometric heterolytic hydrogenation of a carbonyl complex under 1.0 atm of H_2 in the presence of an appropriate base, as shown in Scheme 7, reactions (22)−(24).[36] A similar approach has been used to develop methods for heterolytic cleavage of H_2 in the presence of a base to form B−H bonds directly from H_2 gas using rhodium and cobalt diphosphine complexes.[38,39,59]

Scheme 7. Heterolytic Hydrogenation of a Carbonyl Complex

$\Delta G°$

$H_2 + [Pt(dmpp)_2]^{2+} + Base \rightarrow [HPt(dmpp)_2]^{+} + HBase^{+}$ 0.0 kcal/mol (22)

$HPt(dmpp)_2]^{+} + [Cp*Re(NO)(CO)_2]^{+} \rightarrow$

$Cp*Re(NO)(CO)(CHO) + [Pt(dmpp)_2]^{2+}$ -1.6 kcal/mol (23)

$[Cp*Re(NO)(CO)_2]^{+} + H_2 + Base \rightarrow$

$Cp*Re(NO)(CO)(CHO) + HBase^{+}$ -1.6 kcal/mol (24)

Base = proton sponge®

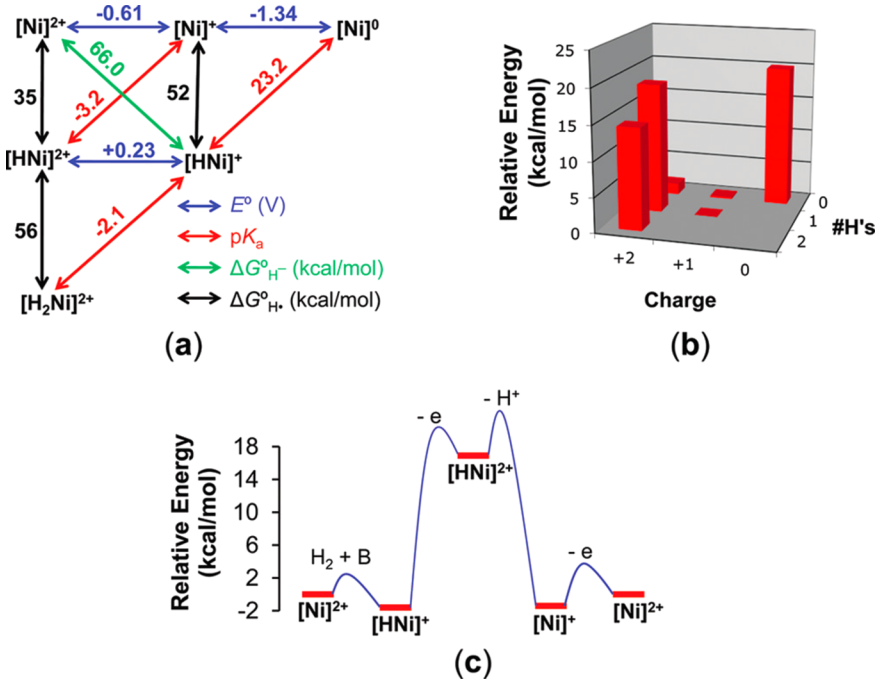

Figure 8. (a) Thermodynamic diagram for the $[Ni(depp)_2]^{2+}$ system in acetonitrile, calculated from the experimental values of two one-electron redox potentials, $E°$(I/0) and $E°$(II/I), using the equations in Figure 7. (b) Free-energy landscape showing the relative free energies of species derived from Ni−H bond cleavage of $[H_2Ni(depp)_2]^{2+}$ (1 atm of H_2 and pH 8.5 in acetonitrile). (c) Free-energy profile for the electrocatalytic oxidation of H_2 ($H_2 + 2B \rightarrow 2HB^{+} + 2e^{-}$, where B denotes a base) by the $[Ni(depp)_2]^{2+}$ catalyst. In part c, the free energies of the individual intermediates (red lines) are accurate, but the blue lines are only a guide to the eye and do not represent the actual activation barriers.

dx.doi.org/10.1021/ic4026969 | Inorg. Chem. 2014, 53, 3935−3960

Each of the aspects of the reactivity of transition-metal hydrides discussed in the preceding two paragraphs can be determined by considering two or three thermodynamic properties of these metal complexes. However, as shown for the ideal catalyst in Figure 1, for catalytic reactions, we are interested in matching the free energies of many intermediates. Of particular interest is the use of thermodynamic diagrams such as that shown in Figure 8a for the $[\mathbf{Ni(depp)_2}]^{2+}$ system in acetonitrile to construct a free-energy map or landscape (Figure 8b) and reaction profile (Figure 8c) for the oxidation of H_2. The value of each of the thermodynamic parameters shown in the free-energy diagram of Figure 8a can be calculated from the two experimentally measured redox potentials for the $Ni^{II/I}$ and $Ni^{I/0}$ couples (−0.61 and −1.34 V, respectively, versus the ferrocenium/ferrocene couple) and the equations shown in Figure 7. From this diagram and thermodynamic cycles, similar to those shown in Schemes 3 and 4, the free-energy landscape shown in Figure 8b can be calculated for specific pH values and H_2 pressures (in this case, 1.0 atm of H_2 and pH 8.5 in acetonitrile). The free-energy landscape in Figure 8b can, in turn, be used to construct the reaction profile (Figure 8c) for the electrocatalytic oxidation of H_2 using $[Ni(depp)_2]^{2+}$ as the catalyst. In this reaction profile, the relative free energies of the intermediates indicated in the catalytic cycle are taken from Figure 8b, but the barriers between these intermediates are arbitrary and are shown only for purposes of illustration. From the reaction profile shown in Figure 8c, it can be seen that the nickel(III) hydride complex $[HNi(depp)_2]^{2+}$ $[\mathbf{HNi}]^{2+}$ is a high-energy intermediate, but the remaining intermediates have similar energies, as is desired for an efficient catalytic process. To improve the efficiency of this catalyst, the energy of the $[\mathbf{HNi}]^{2+}$ intermediate needs to be lowered or the oxidation of this species needs to be coupled with proton transfer to a base.

CONTROLLING PROTON MOVEMENT

Pendant Amines in Molecular Electrocatalysts for H_2 Oxidation and Production. There were a number of considerations that led to another shift in the focus of our research efforts from understanding the thermodynamics of metal hydrides to trying to control the movement of protons during electrocatalytic reactions. First, the high energy of the electrochemically generated intermediate $[\mathbf{HNi}]^{2+}$ (Figure 8c) suggested the incorporation of pendant bases in the second coordination sphere to facilitate proton transfer between the metal center and acids or bases in solution. This coupling of proton-transfer reactions with electron-transfer reactions could avoid significant concentrations of high-energy intermediates such as $[\mathbf{HNi}]^{2+}$. Second, structural, spectroscopic, and theoretical studies of the [FeFe]hydrogenase enzymes suggested that an azadithiolate ligand is present in the active site (structures **1** and **2**) and that this pendant amine plays important roles in H_2 cleavage and proton transfer between the metal center and a proton channel that leads to the surface of the enzyme.[3,60] Finally, a number of studies of protic/hydridic interactions in transition-metal hydrides support the hypothesis that such interactions can play an important role in H_2 activation.[61−64]

The possibility of pendant bases facilitating a variety of crucial steps such as proton-transfer reactions, the coupling of proton- and electron-transfer steps (PCET), and the heterolytic cleavage/formation of the H−H bond prompted us to study a series of nickel diphosphine complexes (Scheme 8, structures $\mathbf{17}^{2+}$−$\mathbf{20}^{2+}$) in stoichiometric as well as electrocatalytic reactions for H_2 oxidation and production. These studies were designed to answer some of the following questions. Can pendant amines participate in the coupling of proton- and electron-transfer reactions and reduce OPs? Can pendant amines facilitate heterolytic cleavage of H_2? How important is the positioning of pendant amines versus more flexible ligand structures? What is the optimum number of pendant amines? Do the different possible sites for proton delivery and removal play significant roles in controlling proton movement? How do the substituents on P and N affect the movement of protons? Are structural features of the ligand that are advantageous for one step of a catalytic reaction detrimental for another step, and if so, how can the catalysts be optimized? What is the role of the outer coordination sphere in proton movement, and can it be controlled? Can the concepts developed for H_2 production and oxidation catalysts be generalized to other metals and substrates? Some of the questions have been answered in the research described below, and some are still being investigated.

Studies of H_2 Addition to Ni and Mn Complexes Containing Pendant Amines. Reactions of a series of $[\mathbf{Ni(diphosphine)_2}]^{2+}$ complexes with H_2 are shown in Scheme 8.

Scheme 8. Structures of $[\mathbf{Ni(diphosphine)_2}]^{2+}$ Complexes and Their H_2 Addition Products in Acetonitrile

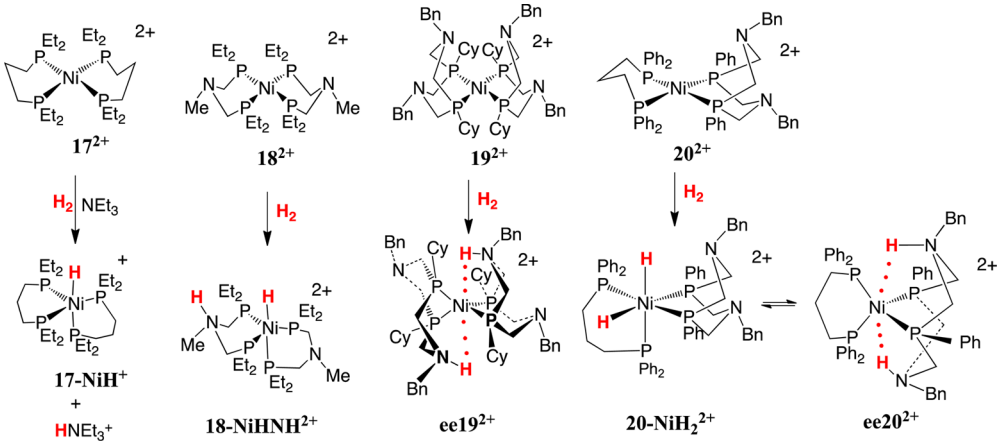

dx.doi.org/10.1021/ic4026969 | Inorg. Chem. 2014, 53, 3935−3960

$[Ni(depp)_2]^{2+}$ (17^{2+}), whose reaction profile is shown in Figure 8c, reacts with H_2 in the presence of triethylamine to form **17-NiH**$^+$ and protonated triethylamine.[35] This reaction involves *intermolecular* heterolytic cleavage of H_2. For complex $[Ni(PNP)_2]^{2+}$ (18^{2+}), the central methylene of the propylene backbone has been replaced with an NMe group, and reaction with H_2 results in *intramolecular* heterolytic cleavage of H_2 to form $[HNi(PNP)(PNHP)]^{2+}$ (**18-NiHNH**$^{2+}$) with a hydride ligand bound to Ni and a proton bound to a N atom of one of the PNP ligands.[65] In contrast, the addition of H_2 to $[Ni(P^{Cy}_2N^{Bn}_2)_2]^{2+}$ (19^{2+}) results in the reduction of Ni^{II} to Ni^0 with formation of **ee19**$^{2+}$ in which a proton is bound to a N atom of each diphosphine ligand.[66,67] In this case, the H atoms on N are endo (**e**) with respect to Ni, and hydrogen bonding with Ni^0 is observed. Later we will discuss isomers of **ee19**$^{2+}$ in which one (**ex19**$^{2+}$) or both N atoms (**xx19**$^{2+}$) are protonated in exo (**x**) positions with N−H···N hydrogen bonding. The addition of H_2 to $[Ni(dppp)(P^{Ph}_2N^{Bn}_2)_2]^{2+}$ results in yet another distribution of the H atoms in the products. At −70 °C, both the dihydride **20-NiH**$_2^{2+}$ and **ee20**$^{2+}$ are observed.[68] The former product is a nickel(IV) *cis*-dihydride species, and the latter is a Ni^0 species in which both protons occupy endo positions on the two N atoms of the $P^{Ph}_2N^{Bn}_2$ ligand. In these complexes, distribution of the protons depends on the relative basicity of the Ni center and the pendant amines.

The first observable species in the reaction of **19**$^{2+}$ with H_2 at −70 °C is the doubly N-protonated Ni^0 complex, **ee19**$^{2+}$.[67] This reaction was studied using DFT calculations to obtain further information on the precise steps involved in H_2 binding and cleavage.[69,70] As can be seen from the calculated reaction pathway shown in Figure 9, the first step involves the formation of a dihydrogen complex (**19-Ni(H$_2$)**$^{2+}$) with an H−H bond distance of 0.80 Å, which lies in a very shallow energy well approximately 4−10 kcal/mol above the reactants, depending on the computational method used. Because the formation of the dihydrogen complex is endergonic, this step contributes to the overall barrier for heterolytic H_2 cleavage. Heterolytic cleavage of H_2, for which the H−H distance of the transition state is 1.02 Å (first transition state in Figure 9), results in the formation of a nickel hydride species (**e19-NiH**$^{2+}$; H−H distance = 1.78 Å) with a protonated pendant amine. This proton hydride species is unstable with respect to transfer of a proton from Ni to N, to form the experimentally observed species **ee19**$^{2+}$ (H−H distance = 3.99 Å). The doubly protonated Ni^0 species **ee19**$^{2+}$ lies in an energy well with respect to H_2 and **19**$^{2+}$, but it is not required for H−H bond heterolysis (or catalysis). Although **19**$^{2+}$ is a good catalyst for H_2 oxidation, the H_2 (**19-Ni(H$_2$)**$^{2+}$) and doubly protonated Ni^0 species (**ee19**$^{2+}$) are too high and too low in energy, respectively, for the most efficient catalytic process.

The stability of the rare nickel(IV) dihydride complex **20-NiH**$_2^{2+}$ is due, in part, to the large dihedral angle between the two diphosphine ligands, as indicated by the large difference in the $Ni^{II/I}$ and $Ni^{I/0}$ potentials of **20**$^{2+}$ (0.54 V).[68] As discussed above, large dihedral angles favor the formation of *cis*-dihydride complexes. For complex **19**$^{2+}$ with cyclohexyl substituents on P and benzyl substituents on N, the nickel(IV) *cis*-dihydride species lies approximately 10−15 kcal/mol higher in energy than the proton hydride species shown in Figure 9.[70] Although computations on the addition of H_2 to **20**$^{2+}$ have not been performed, it is expected that a major difference from the reaction profile shown in Figure 9 will be the presence of a much more stable *cis*-dihydride species, **20-NiH**$_2^{2+}$.

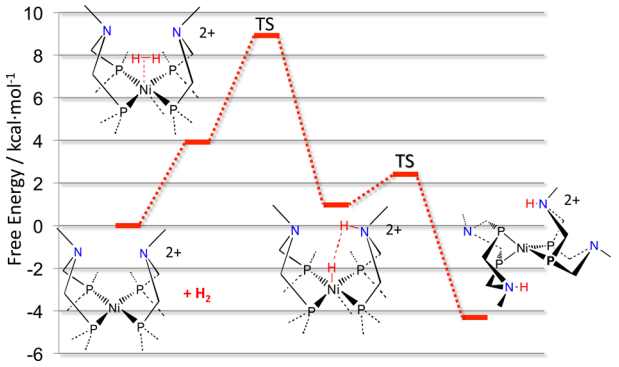

Figure 9. Reaction profile for the addition of H_2 to **19**$^{2+}$. Computational details: DFT/PBE/{Ni(sdd); P, N,C, H(6-31G*); H_2(6-31G**)}; harmonic estimates of free energy with a continuum description of the solvent (cpcm); dispersion correction (Grimme). The *NWChem* and *Gaussian03* programs were used.

The addition of H_2 to the Mn complexes **21**$^+$ and **22**$^+$ (Scheme 9) results in the formation of a H_2 complex, **21-Mn(H$_2$)**$^+$, or a heterolytic cleavage product, **e22-MnH**$^+$.[71,72] As can be seen by a comparison of complexes **21**$^+$ and **22**$^+$, the N atoms of the PNP or $P^R_2N^{R'}_2$ ligands coordinate to the metal in some complexes but not in others, and in solution, there is often an equilibrium between these structures. The vacant coordination site may also participate in agostic interactions involving either the substituents on N or P. An interesting difference between the Ni and Mn complexes is that the latter tend to bind ligands such as acetonitrile irreversibly even at very low concentrations, which prevents H_2 binding in these coordinating solvents. In contrast, the Ni complexes bind acetonitrile reversibly, and H_2 adds easily in this solvent to form the complexes shown in Scheme 8.[65−68] The higher affinity of the Mn complexes for H_2 results in more stable H_2 complexes, but this increased affinity for weakly coordinating ligands also requires the use of weakly coordinating solvents such as fluorobenzene or dichloromethane for electrocatalytic studies, and these catalysts are more easily poisoned or inhibited by impurities.[72]

Studies of Intramolecular Proton Exchange for Ni and Mn Complexes Containing Pendant Amines. Two

Scheme 9. Structures of Mn Complexes and Their H_2 Addition Products in Fluorobenzene or Dichloromethane-d_2 [Where Ar^F = 3,5-Bis(trifluoromethyl)phenyl]

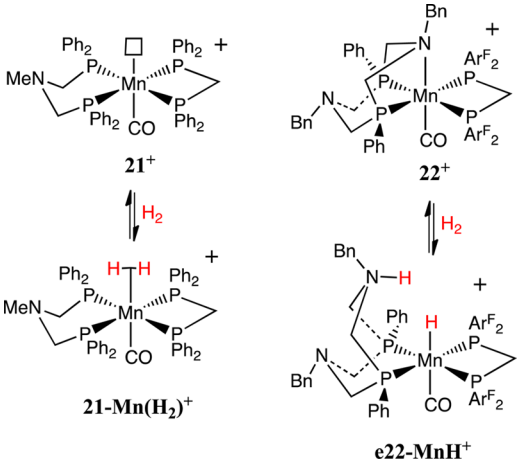

dx.doi.org/10.1021/ic4026969 | Inorg. Chem. 2014, 53, 3935−3960

different types of intramolecular exchange can be observed for the products of H_2 addition to metal complexes containing diphosphine ligands with pendant amines. For Ni complexes, these exchange processes involve proton transfer between Ni and the pendant amine. For example, the hydride ligand of **18-NiHNH**$^{2+}$ in Scheme 8 exchanges with the proton on the pendant amine at a rate of approximately 10^4 s^{-1} in dichloromethane solutions at room temperature.[65] This exchange process could involve any of the three intermediates **18-NiH$_2$**$^{2+}$, **18-Ni(H$_2$)** $^{2+}$, or **18-Ni(NH)$_2$**$^{2+}$, as shown in Scheme 10, but DFT calculations favor **18-Ni(NH)$_2$**$^{2+}$.[73] Similarly, for **ee19**$^{2+}$, the protons bound to the pendant amines migrate from one N atom to the other N atom of the same $P^{Cy}_2N^{Bn}_2$ ligand at a rate of 1.2×10^4 s^{-1} at 298 K in acetonitrile ($\Delta G^{\ddagger}$ = 12 kcal/mol). Detailed NMR and DFT studies indicate that this process occurs by transfer of a proton from one N atom to a fluxional Ni center followed by a second proton transfer from Ni to the other N atom of the same $P^{Cy}_2N^{Bn}_2$ ligand, the last step in Figure 9.[74] The largest contributions to the barrier associated with this process arise from the chair/boat conformational changes of the two six-membered rings (7−10 kcal/mol). Similarly, the two isomers, **20-NiH$_2$**$^{2+}$ and **ee20**$^{2+}$, resulting from H_2 addition to **20**$^{2+}$ are in equilibrium with each other with a rate of exchange of 10−100 s^{-1} at −20 °C in dichloromethane-d_2.[68] This very interesting exchange process that interconverts Ni^0 and Ni^{IV} complexes occurs by two sequential proton transfers between Ni and the N atoms of the pendant amine. The rapid intramolecular exchange observed for all H_2 adducts studied to date involve proton transfers between the Ni center and the pendant amines of the ligand, and they require the basicities of the metal and pendant amines to be similar.

Scheme 10. Possible Intermediates in the Intramolecular Exchange of Hydride and Protons for 18-NiHNH^{2+}

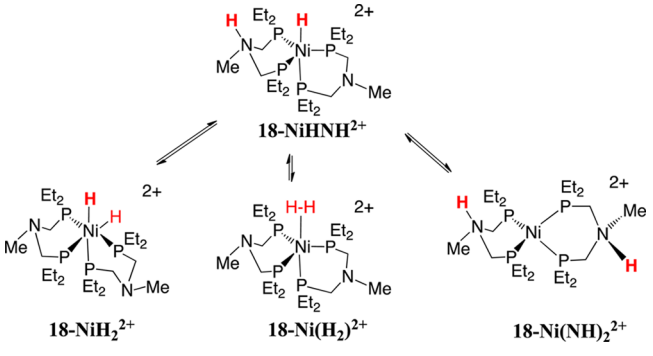

Irreversible deprotonation of the H_2 addition products of **18**$^{2+}$ and **19**$^{2+}$ of Scheme 8 leads to the corresponding $[HNi(PNP)_2]^+$ (**18-NiH**$^+$) and $[HNi(P^{Cy}_2N^{Bn}_2)_2]^+$ (**19-NiH**$^+$) complexes.[65,67] For these hydride complexes, proton transfer between the Ni center and the pendant amines of the ligand may be facile, but it is not experimentally observable. However, deprotonation of the H_2 addition products of **20**$^{2+}$ leads to the formation of **e20**$^+$, *endo*-$[Ni(dppp)(P^{Ph}_2N^{Bn}NH^{Bn})]^+$ [where dppp is bis(diphenylphosphino)propane], a Ni^0 complex with an endo-protonated pendant amine.[68] For this complex, the proton transfers rapidly from one pendant amine to the other via the Ni center with a rate constant of greater than 10^4 s^{-1} at 10 °C. This observation suggests that proton transfer between Ni and the pendant amines is also facile for **18-NiH**$^+$ and **19-NiH**$^+$ and that rapid proton movement between the Ni center and the pendant amines does not cease upon a single deprotonation of H_2 addition products.

Similar to **18-NiHNH**$^{2+}$, rapid intramolecular exchange between the hydride ligand and the protonated pendant amine is also observed for the Mn complex **e22-MnH**$^+$.[72] This exchange involves proton transfer between the hydride ligand and the pendant amine with rapid H−H bond formation to form H_2 complexes similar to **21-Mn(H$_2$)**$^+$ followed by H_2 rotation and H−H cleavage. This differs from the Ni systems, for which proton transfer occurs between the pendant amine and the Ni center rather than a hydride ligand. The different pathway for intramolecular exchange for Mn complexes compared to Ni complexes is attributed to more stable H_2 complexes for Mn compared to extremely rare H_2 complexes for Ni.[75,76] The Mn complex **e22-MnH**$^+$ undergoes proton/hydride exchange at a rate greater than 1.5×10^4 s^{-1} at −95 °C in dichloromethane-d_2.[72] This rate suggests a free energy of activation of less than 6.8 kcal/mol and a rate of at least 6×10^7 s^{-1} at 25 °C. A barrier for H−H bond cleavage of 6 kcal/mol has been calculated for a similar Fe complex, $[CpFe(P^{Ph}_2N^{Bn}_2)(H_2)]^+$, using DFT.[77] Reversible heterolytic cleavage cannot be studied by NMR spectroscopy for H_2 complexes such as$[CpFe(P^{Ph}_2N^{Bn}_2)(H_2)]^+$ and **21-Mn(H$_2$)**$^+$. However, these complexes catalyze the conversion of mixtures of H_2 and D_2 gases to HD. These studies demonstrate that reversible heterolytic cleavage and the formation of a strong H−H bond can be extremely fast for complexes with positioned pendant amines.

Our understanding of the factors required for rapid intramolecular proton exchange between the pendant amine and the hydride ligand is enhanced by studies of complexes for which intramolecular proton exchange is slower than that observed for **e22-MnH**$^+$. For example, **e23-FeH**$^+$ (Scheme 11) undergoes proton/hydride exchange at a rate of 7.3 s^{-1} at −60 °C corresponding to a free energy of activation of 12 kcal/mol and an estimated rate of 1×10^4 s^{-1} at 25 °C.[78] The lower barrier observed for **e22-MnH**$^+$ results, in part, from the presence of a positioned pendant base that does not require chair/boat interconversion (first step in Scheme 11) for H−H bond formation and cleavage. In contrast, chair/boat

Scheme 11. Hydride/Proton Exchange for e23-FeH^{2+}

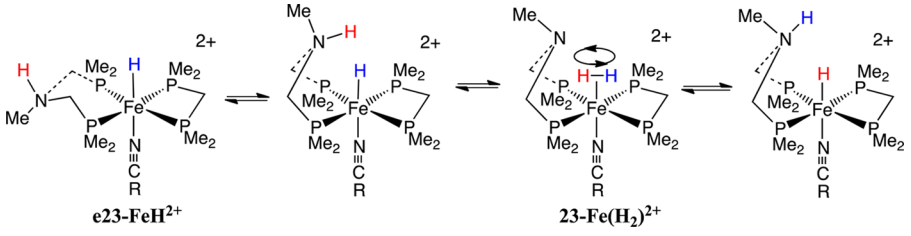

dx.doi.org/10.1021/ic4026969 | Inorg. Chem. 2014, 53, 3935−3960

interconversion must occur during hydride/proton exchange for **e23-FeH**$^{2+}$ because the chair conformation for the resting state of this complex is 5−6 kcal/mol more stable than the boat conformation.

An even more extreme example is observed for the complex **e24-FeH(NH)**$^{3+}$, for which no intramolecular proton exchange is observed by NMR spectroscopy, although the ligand sets for **e23-FeH**$^{2+}$ and **e24-FeH(NH)**$^{3+}$ are very similar in terms of their electronic properties.[79] The failure to observe exchange for **e24-FeH(NH)**$^{3+}$ can be traced to steric interactions between the ethyl substituents on *cis*-PNP ligands that prevent the PNHP ligand cis to the hydride ligand from adopting a boat conformation required for proton/hydride interaction and H−H bond formation. Failure to observe proton/hydride exchange can also be the result of electronic effects. When the acetonitrile ligand in **e23-FeH**$^{2+}$ is replaced with CO, no intramolecular exchange is observed.[78] A *trans*-CO results in less negative charge on the hydride ligand, and movement of a proton from the N atom of the PNP ligand to form the very acidic H_2 complex becomes energetically unfavorable. Thus, optimal rates of intramolecular proton/hydride exchange are expected for Fe and Mn complexes with positioned pendant amines and for which the pK_a values of the protonated pendant amine and the H_2 ligand are matched.

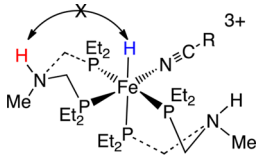

e24-FeH(NH)$^{3+}$

Observation of Isomers Reflecting Different Protonation Sites in Ni and Mn Complexes. The initial products of H_2 addition to the Ni and Mn complexes shown in Schemes 8 and 9 rearrange to form an equilibrium distribution of isomers, as shown in Scheme 12 for **ee19**$^{2+}$.[67,80] Intermolecular deprotonation of **ee19**$^{2+}$ followed by reprotonation in an exo position (as indicated by the designation **x**) leads to the sequential formation of **ex19**$^{2+}$ and **xx19**$^{2+}$. Although there is no distinction between endo and exo protonation sites for the Ni complexes containing the PNP ligand, isomers are observed for Ni complexes with $P^R_2N^{R'}_2$ ligands and for all Mn and Fe complexes with either PNP or $P^R_2N^{R'}_2$ ligands. Endo protonation indicates protonation of the amine ligand such that the proton is adjacent to either a metal center or a hydride ligand.

Hydrogen-Bonding Interactions in the First and Second Coordination Spheres. Protonation of Ni-$(P^{tBu}_2N^{Bn}_2)_2$ with 2 equiv of acid produces **ee**$^{2+}$, **ex**$^{2+}$, and **xx**$^{2+}$ isomers that are of nearly equal energy (within 2 kcal/mol of each other).[81] However, as shown by the potentials listed at the bottom of Scheme 12, the **xx**$^{2+}$ isomer is easier to oxidize than the **ex**$^{2+}$ isomer, and the **ee**$^{2+}$ isomer is the most difficult to oxidize. For the **ee**$^{2+}$ isomer, two $Ni^0\cdots H$ hydrogen bonds are broken upon oxidation of Ni^0 to Ni^I. For the **ex**$^{2+}$ isomer, one $Ni^0\cdots H$ bond is broken upon oxidation to Ni^I, and for the **xx**$^{2+}$ isomer, no $Ni^0\cdots H$ hydrogen bonds are broken upon oxidation. The difference in the oxidation potentials of the **ex**$^{2+}$ and **xx**$^{2+}$ isomers corresponds to the $Ni^0\cdots H$ bond energy of the **ex**$^{2+}$ isomer, 7.4 kcal/mol, and the sum of the free energies of the two $Ni^0\cdots H$ hydrogen bonds in the **ee**$^{2+}$ isomer is 11.3 kcal/mol. The difference in the oxidation potentials of the **ee**$^{2+}$, **ex**$^{2+}$, and **xx**$^{2+}$ isomers for several different complexes indicates that the strengths of these $Ni^0\cdots H$ bonds depend on the substituents on both P and N, with a range of 6.3−9.5 kcal/mol for the **ex**$^{2+}$ isomer. Although hydrogen bonding has not been studied in as much detail for the Fe and Mn complexes as for the Ni complexes, hydrogen bonding appears to involve interactions between a proton bound to a pendant amine and a hydride ligand or between the lone pair of the pendant amine and a H_2 ligand.[72,77] These hydrogen bonds can contribute significantly to the barriers for isomer interconversions discussed in the next section on intermolecular exchange.

Studies of Intermolecular Proton Exchange for Ni Complexes Containing Pendant Amines. In the absence of an exogenous base or water, the rates of interconversion for isomers such as those shown in Scheme 12 are slow. For example, **ee19**$^{2+}$ equilibrates with **ex19**$^{2+}$ over a period of approximately 5 h, while the equilibration of **ex19**$^{2+}$ and **xx19**$^{2+}$ requires approximately 70 h; that is, the **ee19**$^{2+}$/**ex19**$^{2+}$ interconversion is 1 order of magnitude faster than the **ex19**$^{2+}$/**xx19**$^{2+}$ interconversion.[80] Both of these exchange

Scheme 12. Intermolecular Proton Exchange and Isomerization of ee19^{2+} **in Acetonitrile with Base = Aniline**[a]

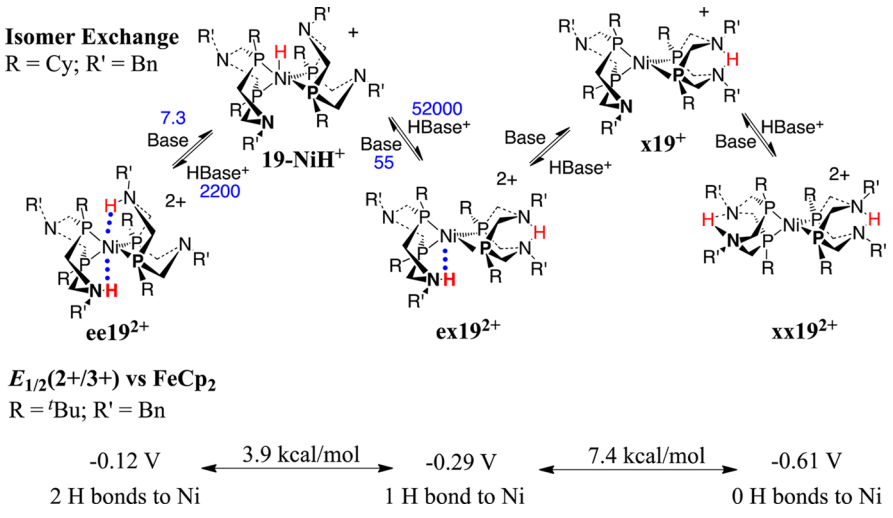

[a]Numbers shown in blue are second-order rate constants (M^{-1} s^{-1}) for the reactions indicated.

dx.doi.org/10.1021/ic4026969 | Inorg. Chem. 2014, 53, 3935−3960

processes are enhanced by the addition of a base such as aniline (pK_a = 10.6 in acetonitrile), as shown by the second-order rate constants indicated in blue in Scheme 12, and further enhancements in rates are seen with the addition of both base and water. The addition of base and/or water does not significantly change the equilibrium distribution of isomers, indicating that neither water nor a weak base disrupts the intramolecular hydrogen bonding in these isomers. The slower rate of interconversion of **ex19**$^{2+}$ and **xx19**$^{2+}$ compared to that of **ee19**$^{2+}$ and **ex19**$^{2+}$ arises because **19-NiH**$^{+}$ is 4−5 kcal/mol more stable than **x19**$^{+}$ (i.e., Ni^0 is more basic than a tertiary amine), which contributes to a similar difference in the activation barriers for these two processes. The faster rates of exchange of **19-NiH**$^{+}$ with **ex19**$^{2+}$ than **ee19**$^{2+}$ result from the greater steric interactions associated with aniline or anilinium accessing an endo site compared to an exo site. These studies indicate that the rate of intermolecular exchange is largely determined by the following factors: (1) how well the pK_a values of the exogenous base and the pendant amine are matched, (2) the size of the substituents on N and P and the size of the exogenous acid or base, (3) the strength of the Ni^0···H hydrogen bonds and hydrogen bonds between the two pendant amines on the same ligand, and (4) the strength of the hydrogen bond between the protonated pendant amine and the exogenous base. The acceleration of the rates of isomer interconversion observed upon the addition of water is attributed to its ability to act as a relay by bridging between the exogenous base or acid and the pendant amine.[82] This partially avoids the costly steric interactions between the P substituents and the exogenous base or acid. This point is under further study using DFT and molecular dynamics calculations.

The kinetic product of H_2 addition to **19**$^{2+}$ is the endo/endo isomer, **ee19**$^{2+}$.[67,80] In contrast, protonation of the Ni^0 complex **19** with 2 equiv or more of acid leads to approximately 95% formation of the **xx19**$^{2+}$ isomer.[80] Similarly, protonation of the nickel hydride **19-NiH**$^{+}$ leads to the nearly quantitative formation of **ex19**$^{2+}$. Thus, exo protonation is kinetically favored for these Ni complexes with pendant amines. Darensbourg and co-workers have observed similar kinetic preferences when [Pt(PTA)$_4$] (where PTA is 1,3,5-triaza-7-phosphaadamantane) is protonated with strong acids at the PTA ligands (the kinetic product) and at Pt for weak acids (the thermodynamic product).[83] The observation of different kinetic and thermodynamic products has significant implications for the rates and pathways of electrocatalytic H_2 production and oxidation by [Ni($P^R_2N^{R'}_2$)]$^{2+}$ catalysts, as discussed in more detail below.

The two preceding paragraphs describe intermolecular proton-exchange processes for Ni complexes containing $P^R_2N^{R'}_2$ ligands. The observation of average chemical shifts for both ^{31}P and ^{1}H NMR resonances during experiments to determine the pK_a value for **18-NiHNH**$^{2+}$ using anisidine as the base indicates an intermolecular exchange process with a second-order rate constant greater than 10^6 M^{-1} s^{-1}, larger than those observed for the **ee19**$^{2+}$, **ex19**$^{2+}$, and **xx19**$^{2+}$ isomers shown in Scheme 12.[65,80] This suggests that pendant amines in the latter complexes, with their hydrogen bonds to Ni^0 or to the second amine in the ligand backbone, undergo slower rates of intermolecular exchange than their more flexible PNP analogues. For Ni complexes, a positioned pendant amine in $P^R_2N^{R'}_2$ ligands facilitates H_2 cleavage and intramolecular proton exchange between the metal and the pendant amine better than the more flexible PNP ligands, but it hinders direct intermolecular proton exchange with acids or bases in solution.

In addition to intermolecular exchange between the H_2 addition products, intermolecular exchange is also observed for their deprotonated analogues. For example, a strong exchange cross-peak is observed between the hydride ligand of **18-NiH**$^{+}$ and H_2O at mixing times as short as 0.1 s for NOESY experiments in acetonitrile solutions at room temperature.[65] In contrast, when D_2O is added to the analogous [HNi(depp)$_2$]$^{+}$ complex, which lacks a pendant amine, less than 10% incorporation of deuterium is observed after 48 h. This corresponds to a difference in rates of at least 10^6. These observations support the importance of the pendant amine of the diphosphine ligand for the rapid intermolecular proton exchange observed for [HNi(PNP)$_2$]$^{+}$. One possible mechanism for this exchange process involves protonation of the pendant amine followed by intramolecular proton/hydride exchange, as shown in Scheme 10 and discussed above. However, the differences in the pK_a values of water and the protonated pendant amines are large, suggesting a large energy barrier for such a process. A possible mechanism that does not require chair/boat interconversion or protonation of a pendant amine by water is suggested by structure **25**$^{+}$. For this structure, intermolecular proton exchange occurs via a concerted formation of Ni−H and O−H bonds involving a water molecule that hydrogen bonds with a pendant amine. Thus, pendant amines are thought to enhance the rates of intermolecular exchange of a proton on water with the hydride ligand of metal hydride complexes by the favorable positioning of a water molecule in close proximity to the hydride ligand and the metal center.[79]

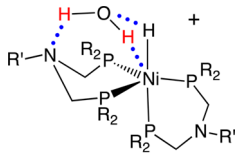

25^{+}

Role of Pendant Amines in PCET Reactions. As discussed above, studies of [HNi(diphosphine)$_2$]$^{+}$ complexes have led to eq 25, which accurately predicts the oxidation potentials of the NiH$^{III/II}$ couples, $E°$(III/II), for complexes without a pendant amine.[55]

$$E°(\mathrm{III/II}) = 1.02E°(\mathrm{I/0}) + 1.60 \qquad (25)$$

Using this relationship leads to the prediction that [HNi($P^{tBu}_2N^{Bn}_2$)$_2$]$^{+}$ should oxidize at +0.55 V compared to the observed potential of −0.67 V, or 1.22 V more negative than expected. This large shift in the potential arises from an intramolecular PCET reaction. As shown in Scheme 13, this PCET process could occur by PTET, ETPT, or EPT. Theoretical calculations by the Hammes-Schiffer group for [HNi($P^{Me}_2N^{Me}_2$)$_2$]$^{+}$ and [HNi($P^{Ph}_2N^{Bn}_2$)$_2$]$^{+}$ complexes suggest that this reaction proceeds through an ETPT process.[84] However, this may change with the structure of the complex. For example, in the mixed-ligand complex *endo*-[Ni(dppp)($P^{Ph}_2NH^{Bn}N^{Bn}$)]$^{+}$ (**e20**$^{+}$), the proton is bound to N in an endo position and not to Ni.[68] This suggests a small barrier to proton transfer from Ni to N for some hydride complexes and a PTET mechanism for the oxidation of **NiH**$^{+}$ intermediates. An interesting suggestion made in the Hammes-Schiffer studies is that the mechanism for electron and proton transfer would

dx.doi.org/10.1021/ic4026969 | Inorg. Chem. 2014, 53, 3935−3960

become concerted if N and Ni could approach each other more closely. A remaining question is, how fast are the intramolecular proton-transfer reactions that accompany the electron-transfer reactions? The large potential shifts suggest rates of intramolecular proton transfer much faster than those observed for species such as **18-NiHNH**$^{2+}$ and **ee19**$^{2+}$, which occur with first-order rate constants of 10^4–10^5 s^{-1}.[65,80]

Scheme 13. Possible Mechanisms for PCET Reactions of NiH^{+}[a]

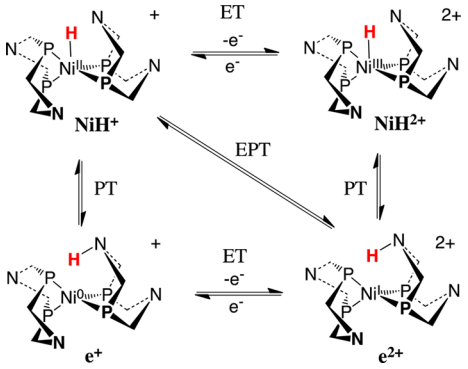

[a]Substituents on P and N are not shown.

Although the largest contribution to the potential shift of the $NiH^{III/II}$ couples is the coupling of intramolecular proton transfer from Ni to N with electron transfer to the electrode, intermolecular proton transfer can contribute as well. For example, not only does the $NiH^{III/II}$ couple for **18-NiH**$^{+}$ shift because of the presence of an internal base, but an additional potential shift is observed in the presence of an exogenous base, as a result of an intermolecular PCET process.[65] Thus, both intra- and intermolecular PCET reactions can contribute to the negative potential shifts observed for the oxidation of nickel hydride intermediates.

Structure and Dynamics of Electrocatalysts in Different Oxidation States. The pendant amines play important roles in intra- and intermolecular proton-transfer reactions, heterolytic cleavage and heteroformation of the H–H bond, and in PCET reactions for the Ni catalysts described above. However, there are other structural and dynamic processes that accompany electrocatalytic reactions. During each catalytic cycle, these catalysts access different oxidation states and structures. $[Ni^{II}(diphosphine)_2]^{2+}$ complexes typically exhibit Ni–P bond distances of approximately 2.20 Å and dihedral angles of 0–30° between the two planes formed by the P atoms of each diphosphine ligand and Ni, depending on the steric bulk of the substituents on P and the chelate bite angle.[31] In solution, these four-coordinate square-planar Ni^{II} complexes can coordinate a solvent molecule such as acetonitrile to form square-pyramidal or trigonal-bipyramidal complexes. Upon reduction from Ni^{II} to Ni^{I}, Ni–P bond distances change very little, with Ni^{I}–P bond distances between 2.21 and 2.23 Å.[81] However, the overall geometry changes from a square-planar or five-coordinate complex to a distorted tetrahedral structure with a dihedral angle between the diphosphine ligands of approximately 85°. Protonation of pendant amines will therefore involve different steric interactions in the Ni^{II} and Ni^{I} oxidation states. Reduction from Ni^{I} to Ni^{0} produces little change in the overall tetrahedral geometry but a significant contraction in bond distances. Ni^{0} complexes have distorted tetrahedral geometries with dihedral angles close to 90°, and the Ni–P bond distances are typically 2.13 to 2.15 Å, or 0.08 to 0.12 Å shorter than Ni^{I}–P distances.[31,81] Finally, during proton transfer between the endo-protonated pendant amine of the ligand and the Ni center for **ee**$^{2+}$ and **ex**$^{2+}$ complexes, the formal oxidation state of Ni changes from Ni^{0} to Ni^{II}, and this is reflected in a change in the Ni–P bond distances. A typical Ni–P distance for a nickel hydride complex is 2.20 to 2.22 Å compared to a Ni–P distance of 2.13–2.15 Å for a Ni^{0} complex. Associated with these structural changes are reorganization energies for both the complex and solvent that contribute to activation barriers for both electron- and proton-transfer reactions.

In addition to the structural changes resulting from the catalyst cycling between oxidation states, other dynamic processes associated with these Ni complexes include boat/chair conformational changes of each of the four rings. For $[Ni(P^{R}{}_2N^{R'}{}_2)_2(CH_3CN)]^{2+}$ complexes, the rates of these conformational changes range from 10^4 to 10^7 s^{-1} at 25 °C.[80,85] This process occurs through a multistep mechanism, which involves dissociation of the acetonitrile, chair/boat isomerization of each of the four rings, and reassociation of an acetonitrile on the opposite side of the complex, as shown in Scheme 14. Free energies of activation of 4.8, 7.7, and 6.5 kcal/mol were obtained from line-shape analysis of $^{31}P\{^{1}H\}$ NMR spectra of the zerovalent Ni complexes $[Ni^{0}(P^{Cy}{}_2N^{Ph}{}_2)_2]$, $[Ni^{0}(P^{Cy}{}_2N^{Bn}{}_2)_2]$, and $[Ni^{0}(P^{Ph}{}_2N^{Bn}{}_2)_2]$, respectively, for similar boat/chair isomerization processes. For the nickel(II) hydride complexes $[HNi^{II}(P^{Cy}{}_2N^{Ph}{}_2)_2]^{+}$ and $[HNi^{II}(P^{Cy}{}_2N^{Bn}{}_2)_2]^{+}$, free energies of activation of 5.5 and 9.3 kcal/mol, respectively, have been obtained. For Ni^{I} complexes, it is not possible to observe the rates of chair/boat isomerizations by NMR, but it is anticipated that they will be comparable to the Ni^{0} and hydride complexes.

Scheme 14. Conformational and Ligand Exchange for $[Ni(CH_3CN)(P^{R}{}_2N^{R'}{}_2)_2]^{2+}$ Complexes

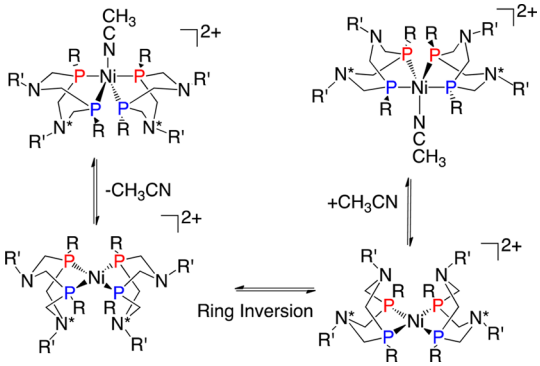

Although the barriers for chair/boat isomerization are generally small, they can contribute significantly to the barriers of more complex intra- and intermolecular exchange processes described above. During the time of a single catalytic cycle, which can range from approximately 1 to 10^{-5} s, significant structural changes occur. These include changes in (1) the bond lengths, coordination numbers, and dihedral angles of the first coordination sphere, (2) chair/boat conformational changes and inversion of N in the second coordination sphere, and (3) proton transfer between the first and second spheres (i.e., the metal center and pendant amine) and between the

dx.doi.org/10.1021/ic4026969 | Inorg. Chem. 2014, 53, 3935–3960

second coordination sphere and solution (i.e., between the pendant amines and acids and bases in solution). The conformational changes and structural changes associated with electron- and proton-transfer reactions contribute to the activation barriers for the different steps involved in catalysis of H_2 oxidation and production.

Ni H_2 Oxidation Catalysts. The preceding sections have discussed the structure and dynamics of the catalysts in different oxidation and protonation states and the role of the pendant amines in a variety of stoichiometric reactions including H_2 binding, H−H bond cleavage and formation, intramolecular proton transfer, intermolecular proton transfer, and PCET reactions. Different combinations of these stoichiometric reactions result in more complex catalytic reactions. Two catalytic cycles for H_2 oxidation by $[Ni(P^{Cy}_2N^{tBu}_2)_2]^{2+}$ are shown in Scheme 15.[86] The reaction of $[Ni(P^{Cy}_2N^{tBu}_2]^{2+}$ (**Ni**$^{2+}$) with H_2 results in the formation of the first experimentally observable intermediate, **ee**$^{2+}$, through a sequence of steps shown in Figure 9. The resulting **ee**$^{2+}$ product can be oxidized or deprotonated. For large bulky bases such as triethylamine, there is a large steric interaction with the ^{t}Bu groups on N and the Cy groups on P. This prevents direct deprotonation and favors oxidation of **ee**$^{2+}$ to form **ee**$^{3+}$, which occurs at −0.36 V versus the ferrocene/ferrocenium couple. Deprotonation of **ee**$^{3+}$ to form **e**$^{2+}$ is thermodynamically easier than deprotonation of **ee**$^{2+}$ because of the increased charge. In addition, the disappearance of Ni···HN hydrogen bonding lengthens the Ni−N distance and provides greater accessibility of the proton on the pendant amine to an exogenous base such as triethylamine. Deprotonation of **e**$^{2+}$ to form **Ni**$^{+}$ and oxidation of the latter to **Ni**$^{2+}$ completes the catalytic cycle.

Scheme 15. Two Pathways for the Electrocatalytic Oxidation of H_2 by Ni^{2+}

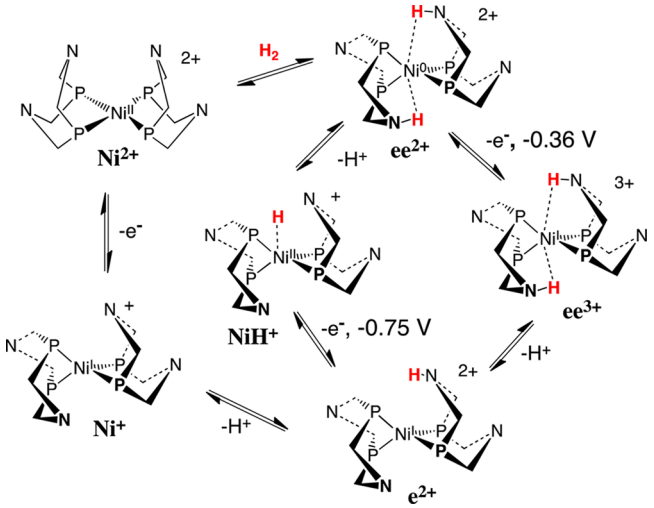

In contrast, a smaller base such as *n*-butylamine or a bulky base such as triethylamine in the presence of water can deprotonate **ee**$^{2+}$ to form the **NiH**$^{+}$ complex, which oxidizes at −0.75 V because of the coupling of intra- and intermolecular proton-transfer reactions with electron transfer.[86] The common intermediate formed in these two pathways, **e**$^{2+}$, can be sequentially deprotonated and oxidized to form the starting **Ni**$^{2+}$ complex. These results illustrate that subtle differences such as the size of the exogenous base or the presence or absence of water can determine the pathway for catalytic H_2 oxidation, with differences in operating potentials of nearly 0.4 V.

The ability of CO to inhibit the catalyst performance is an important consideration because CO is a frequent contaminant in H_2 and CO poisons Pt fuel cells even at ppm levels. Although $[Ni(P^R_2N^{R'}_2)_2]^{2+}$ catalysts react with CO to form five-coordinate complexes (one of which has been characterized by X-ray crystallography), they are not significantly inhibited by concentrations of CO as high as 50% in the presence of 1.0 atm of H_2.[66,86,87] The greater binding affinity of $[Ni(P^R_2N^{R'}_2)_2]^{2+}$ catalysts for H_2 compared to CO is attributed to the different modes of binding. H_2 is split to form two strong N−H bonds with significant hydrogen-bonding interactions either to Ni or a second N atom, whereas CO binds very weakly to the Ni^{2+} center and is weakly stabilized by Coulombic interactions between the lone pairs on two N atoms and the positively charged C atom of CO.

Development of Catalysts for H_2 Production: Controlling the Thermodynamic Driving Force. The thermodynamic cycle shown in Scheme 16 provides a method for determining the driving force for the addition of H_2 to $[Ni(P^R_2N^{R'}_2)_2]^{2+}$ complexes as measured by $\Delta G^\circ_{H_2}$. The hydride donor abilities are determined by the steric and electronic properties of the substituents on P as discussed above, and the pK_a values are determined by the electron donor abilities of the substituents on N. Using these properties, $\Delta G^\circ_{H_2}$ for $[Ni(P^R_2N^{R'}_2)_2]^{2+}$ has been tuned over a range from −7.9 kcal/mol (R = Cy and R′ = ^{t}Bu) to +13.8 kcal/mol (R = Me and R′ = Ph).[86,88] Complexes for which $\Delta G^\circ_{H_2}$ is positive are H_2 production catalysts, and complexes for which $\Delta G^\circ_{H_2}$ is negative are H_2 oxidation catalysts. Two series of H_2 production catalysts have been studied as a function of $\Delta G^\circ_{H_2}$. For $[Ni(P^{Ph}_2N^{C6H4X}_2)_2]^{2+}$ complexes, the TOFs increased from 480 to 1040 s^{-1} as the pK_a of the protonated parent of the pendant amine decreased from 11.9 to 9.4.[82] For a second series of $[Ni(P^R_2N^{Ph}_2)_2]^{2+}$ complexes, the substituents on P were varied, while the phenyl substituent on N remained constant.[88,89] As $\Delta G^\circ_{H^-}$ decreased from 59.0 kcal/mol for R = Ph to 54 kcal/mol for R = Me (or the hydride donor ability increased by 5 kcal/mol), the TOF for H_2 production increased from 720 to 6700 s^{-1}.

Catalysts with values of $\Delta G^\circ_{H_2}$ close to 0 kcal/mol are slower than those with more positive values, but they also operate at much lower OPs. For example, $[Ni(P^{Ph}_2N^{Bn}_2)_2]^{2+}$ ($\Delta G^\circ_{H_2}$ = +2.7 kcal/mol) exhibits a rate of 4 s^{-1} for H_2 production with an OP of 50 mV.[90] Similarly, the catalyst $[Ni(P^{Ph}_2N^{R'}_2)_2]^{2+}$ (where R′ = $CH_2CH_2OCH_3$), for which $\Delta G^\circ_{H_2}$ = +0.84 kcal/mol, is a catalyst for both H_2 production and oxidation.[91] Thus, these synthetic complexes can be tuned for catalytic H_2 oxidation, H_2 production, or reversible catalysis.

Mechanisms of Electrocatalytic Production of H_2 by $[Ni(P^R_2N^{R'}_2)_2]^{2+}$ Complexes. The simplest mechanism for the catalytic production of H_2 by $[Ni(P^R_2N^{R'}_2)_2]^{2+}$ complexes would be the reverse of that observed for H_2 oxidation and is indicated by a counterclockwise rotation in the red dotted box of Scheme 17. In such a cycle, reduction of Ni^{II} complexes to Ni^{I} in acidic acetonitrile solutions would be followed by endo

dx.doi.org/10.1021/ic4026969 | Inorg. Chem. 2014, 53, 3935−3960

Scheme 16. Thermodynamic Cycle Used To Calculate the Driving Force for H_2 Addition to $[Ni(P^R_2N^{R'}_2)_2]^{2+}$ Complexes

$$[Ni(P^{Cy}_2N^{tBu}_2)_2]^{2+} + H^- \leftrightarrows [HNi(P^{Cy}_2N^{tBu}_2)_2]^+ \quad -\Delta G°_{H^-} = -61.3 \text{ kcal/mol}$$

$$[HNi(P^{Cy}_2N^{tBu}_2)_2]^+ + H^+ \leftrightarrows [Ni(P^{Cy}_2N^{tBu}_2H)_2]^{2+} \quad \Delta G° = -1.37(pKa) = -22.6 \text{ kcal/mol}$$

$$H_2 \leftrightarrows H^- + H^+ \quad \Delta G° = 76 \text{ kcal/mol}$$

$$[Ni(P^{Cy}_2N^{tBu}_2)_2]^{2+} + H_2 \leftrightarrows [Ni(P^{Cy}_2N^{tBu}_2H)_2]^{2+} \quad \Delta G°_{H2} = -7.9 \text{ kcal/mol}$$

Scheme 17. Proposed Mechanism of H_2 Formation for $[Ni(P^R_2N^{R'}_2)_2]^{2+}$ Complexes

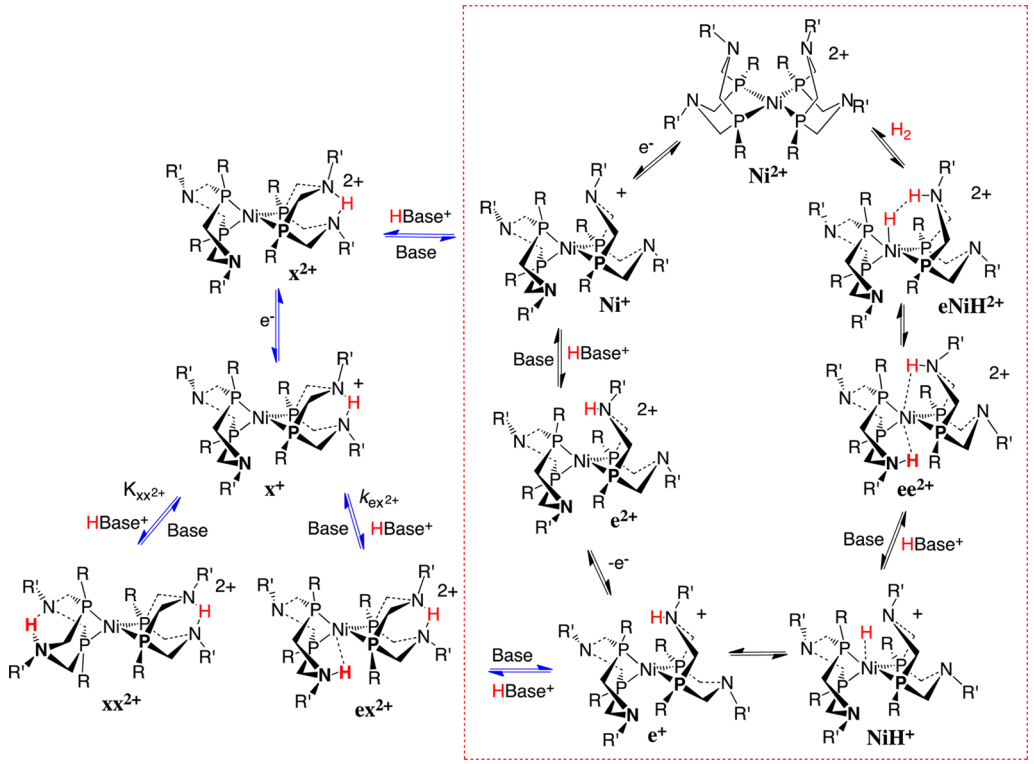

protonation of a pendant amine to form $[Ni(P^R_2N^{R'}_2)(P^R_2N^{R'}_2H)]^{2+}$ ($\mathbf{e^{2+}}$). However, this protonation step may also occur at an exo position to form $\mathbf{x^{2+}}$, and the blue arrows of Scheme 17 indicate an alternative pathway for H_2 production. Protonations of Ni^{II} complexes, such as $[Ni(P^{Ph}_2N^{Bn}_2)_2]^{2+}$, and the Ni^0 complexes, such as $Ni(P^{Ph}_2N^{Bn}_2)_2$ and $Ni(P^{Cy}_2N^{Bn}_2)_2$, occur with greater than 95% selectivity at the exo position.[80,81,86,90] Similarly, protonation of **19-NiH$^+$** occurs at the exo position to form the $\mathbf{ex^{2+}}$ isomer in which the hydride proton has transferred from the Ni center to a N in an endo position.[80] These results indicate that the kinetic product resulting from reduction and protonation of the catalyst is the $\mathbf{xx^{2+}}$ isomer. This isomer is the resting state of the catalyst at potentials negative of the $Ni^{II/I}$ couple. However, only the $\mathbf{ee^{2+}}$ isomer can evolve to eliminate H_2. Under the steady-state conditions observed during catalysis, the experimentally determined rate expression has the following form: rate of H_2 production = $\{(k_{ex^{2+}})(k_{-xx^{2+}})[HBase^+]^2\}[catalyst]/\{k_{-xx^{2+}} + (k_{xx^{2+}})[HBase^+]^2\}$ (see Scheme 17 for corresponding reactions).[67,82,89,90] At high $HBase^+$ concentrations, a pseudo-first-order rate constant $k_{ex^{2+}}/K_{xx^{2+}}$ is observed with no dependence on the $HBase^+$ concentration, and at low $HBase^+$ concentrations, a second-order dependence on $HBase^+$ is observed. As discussed in the section on intermolecular proton exchange, small exogenous acids and bases enhance the rate of isomer interconversion, and the fastest catalytic rates for H_2 production are observed for small acids that increase the rate of endo protonation of $\mathbf{x^+}$ and $k_{ex^{2+}}$. For example, $[Ni(P^{Ph}_2N^{Ph}_2)_2]^{2+}$ has TOFs of 31 and 590 s^{-1} for 2,6-dichloroanilinium and protonated DMF, respectively.[82] Even higher rates are observed when water is added, 160 and 720 s^{-1} for 2,6-dichloroanilinium and protonated DMF, respectively. Water is thought to facilitate proton transfer between the proton of the acid in solution and the endo position of the N atom of a pendant amine by acting as a bridge. These results indicate that reducing steric interactions between the exogenous acid in solution and the substituents on the P atoms enhances the rates of catalytic H_2 production.

To avoid the formation of undesireable $\mathbf{xx^{2+}}$ and $\mathbf{ex^{2+}}$ isomers, a new catalyst, $[Ni(7\text{-}P^{Ph}_2N^{Ph})_2]^{2+}$ ($\mathbf{26^{2+}}$), with one less N atom in each diphosphine ligand was synthesized.[92] As expected, $\mathbf{26^{2+}}$ is an electrocatalyst for the reduction of protons in acetonitrile to produce H_2. However, unlike $[Ni(P^R_2N^{R'}_2)_2]^{2+}$ catalysts, the reactions are first-order in acid over the entire range of acid concentrations studied. Theoretical studies indicate that the pK_a value of $\mathbf{e26^{2+}}$ (the

dx.doi.org/10.1021/ic4026969 | Inorg. Chem. 2014, 53, 3935−3960

protonated form of $\mathbf{26}^{2+}$ after being reduced by one electron) in acetonitrile is 5.9, while the pK_a value of $\mathbf{x26}^{2+}$ is 1.4.[93] Thus, in the presence of $[HDMF]^+$ (pK_a = 6.1), only $\mathbf{e26}^{2+}$ should enter the catalytic cycle, and the bottleneck arising from exo protonation should be removed. This complex exhibits a TOF of 33000 s^{-1} at the maximum acid concentration studied (0.43 M $[H(DMF)]^+$), and the addition of water results in a further increase in the TOF to 106000 s^{-1} (0.43 M $[HDMF]^+$ and 1.2 M H_2O).[92] Although this catalyst functions with a relatively high OP, 625 mV, these results clearly indicate that pendant amine bases in the second coordination sphere are capable of promoting fast proton transfer from solution to the metal center and fast H−H bond formation.

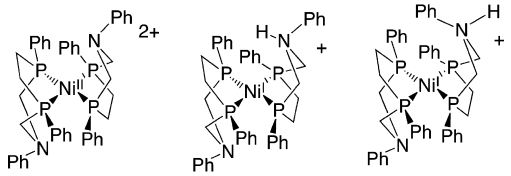

$\mathbf{26}^{2+}$ $\mathbf{e26}^{2+}$ $\mathbf{x26}^{2+}$

Predictive Models, Thermodynamic Diagrams and Free-Energy Landscapes of $[Ni(P^R_2N^{R'}_2)_2]^{2+}$ Catalysts. The thermodynamic models developed previously for $[Ni(diphosphine)_2]^{2+}$ complexes and their derivatives can be extended to $[Ni(P^R_2N^{R'}_2)_2]^{2+}$ complexes. A series of equations, shown in Figure 7, have been developed using DFT calculations for $[Ni(diphosphine)_2]^{2+}$ systems that predict the relative free energies of possible catalytic intermediates from two parameters, the $Ni^{II/I}$ and $Ni^{I/0}$ potentials.[55] A similar, but more extensive, series of equations for $[Ni(P^R_2N^{R'}_2)_2]^{2+}$ systems has also been developed that allows the relative free energies of the 25 possible catalytic intermediates shown in Scheme 18 to be predicted from three parameters, the $Ni^{II/I}$ and $Ni^{I/0}$ couples and the pK_a values of the protonated primary amines from which the $P^R_2N^{R'}_2$ ligands are derived.[94] As in Figure 7, the columns in Scheme 18 represent the charge on the metal complex extending from 4+ on the right to 0 on the left. The rows again represent the number of H atoms attached either to the Ni center or to a pendant amine: zero for the first row, one for the second, and two for the third. The possibility of the H atoms attaching to pendant amines as well as the Ni center results in isomers. For example, instead of only a nickel hydride species, $[HNi(P^R_2N^{R'}_2)_2]^+$ ($\mathbf{NiH}^+$), the endo- and exo-protonated Ni^0 species, $\mathbf{e}^+$ and $\mathbf{x}^+$, are also possible. These isomers lead to the three members shown for each matrix element of the second row. There are also seven isomers of reasonable energy possible for the matrix element corresponding to species with a 2+ charge and containing two H atoms, as discussed in some detail above. For the 3+ and 4+ species containing two H atoms, computational studies indicate that the N-protonated species are of relatively low energy, in agreement with experiment. However, the hydride species are very high in energy and are therefore not considered.

Figure 10 shows a free-energy landscape for the $[Ni(P^{Ph}_2N^{Ph}_2)_2]^{2+}$ system corresponding to the different species shown in Scheme 18. The x (charge) and y (number of H atoms) axes determine the species under consideration, and the relative free energies of each species are shown along the z axis. The relative free energies are dependent on the pH of the solution and on the H_2 pressure. For the example shown, the pressure is 1.0 atm, and the pH of the acetonitrile solution is 6.1. These conditions have been used in previous studies of H_2 production by this catalyst.[67,82,87−89] Two electrons and two protons must be combined during the catalytic process, which could occur by ECEC, ECCE, EECC, CECE, CCEE, or CEEC processes. In these mechanistic descriptions, E represents an electron-transfer step and C represents a proton-transfer step. The latter can occur at endo or exo positions of the N atoms or at the metal center. Thus, the total number of pathways is large. However, the free-energy landscape of Figure 10 can be used to compare and analyze different possible catalytic mechanisms.

It can be seen from Figure 10 that $\mathbf{Ni}^{2+}$ is the most stable species at pH 6.1 and 1.0 atm of H_2, representing the resting state of the catalyst in the absence of an applied potential. Protonation of the $\mathbf{Ni}^{2+}$ species to form $\mathbf{x}^{3+}$ (pK_a = 3.4) or $\mathbf{e}^{3+}$ (pK_a = 1.2) is uphill by 3.7 and 6.7 kcal/mol, respectively, using $HDMF^+$ as the acid. Thus, the free-energy landscape of Figure 10 suggests that electron transfer will be the first step in catalytic H^+ reduction and that catalytic processes beginning with proton transfer, such as the CECE, CCEE, or CEEC mechanisms, will not contribute to catalysis. Experimentally, it

Scheme 18. Thermodynamic Diagram for the $[Ni(P^{Ph}_2N^{Ph}_2)_2]^{2+}$ H_2 Production Catalyst

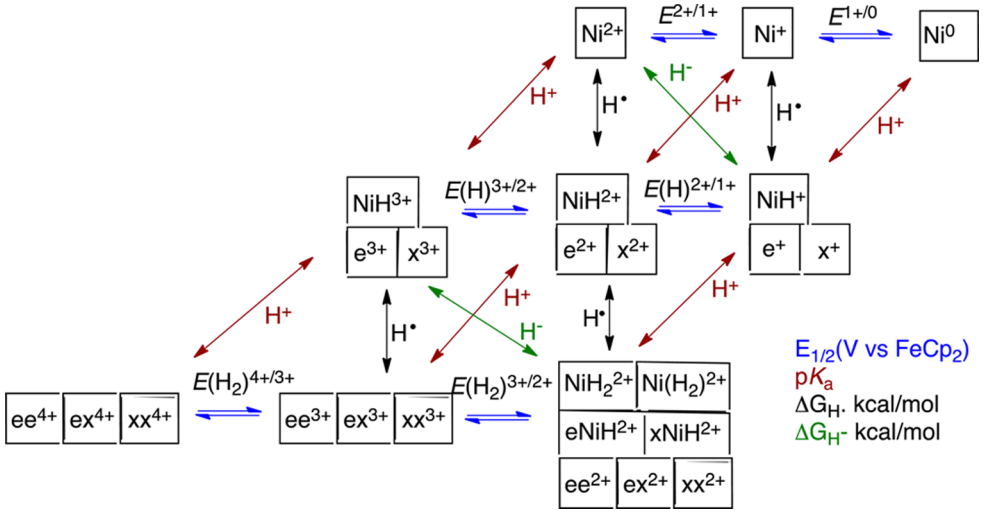

dx.doi.org/10.1021/ic4026969 | Inorg. Chem. 2014, 53, 3935−3960

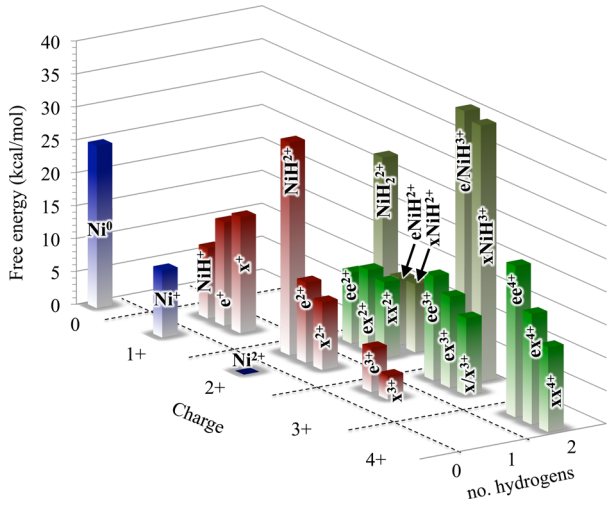

Figure 10. Free-energy landscape for the $[Ni(P^{Ph}_2N^{Ph}_2)_2]^{2+}$ catalyst. The *x* axis indicates the number of H atoms for each species, the *y* axis the charge of each species, and the *z* axis the relative free energies of the different species at pH 6.1 and 1.0 atm of H_2. The labeling used for the different species is the same as that used in Scheme 18. Blue bars represent intermediates with no hydrogen; red bars represent intermediates with one hydrogen; green bars represent intermediates with two hydrogens. This figure has been modified from Figure 7 of ref 94.

is observed that reduction of $\mathbf{Ni^{2+}}$ to $\mathbf{Ni^{+}}$ occurs at −0.83 V with the onset of catalysis. This potential is more negative than the H^+/H_2 couple at pH 6.1 (−0.43 V), and this potential difference of 0.4 V (or 9.2 kcal/mol) corresponds to the OP. This OP is required to change the basicity of the pendant amine so that protonation of the reduced species may occur at the pH of the solution, 6.1.

For an EECC process, a second electron must be transferred to the catalyst, reducing Ni^+ to Ni^0 at a potential of −1.02 V versus the ferrocene/ferrocenium couple or at an OP of 0.59 V. For $[Ni(P^{Ph}_2N^{Ph}_2)_2]^{2+}$, catalysis can proceed via this pathway, but this pathway is associated with the penalty of a larger OP, i.e., a much less efficient pathway. It can also be seen from Figure 10 that, if this catalyst lacked pendant amines, protonation of $\mathbf{Ni^+}$ to form $\mathbf{NiH^{2+}}$ is unfavorable and will not occur under the conditions specified. Reduction of $\mathbf{Ni^{2+}}$ to $\mathbf{Ni^0}$ would be required before protonation at Ni would be favorable. From such considerations, it is obvious that the incorporation of pendant amines provides multiple pathways for H_2 production that avoid the high-energy intermediates ($\mathbf{Ni^0}$, $\mathbf{NiH^{2+}}$, and $\mathbf{NiH_2^{2+}}$) associated with $[Ni(diphosphine)_2]^{2+}$ complexes lacking pendant amines. Analysis of the ECEC catalytic pathway indicated by the blue arrows in Scheme 17 indicates that this is a favorable pathway for H_2 production based on the energies of the catalytic intermediates.[94]

The free-energy landscape shown in Figure 10 is for a specific catalyst and set of conditions, and it can provide insight into potential catalytic pathways. The equations that have been developed for the $[Ni(P^R_2N^{R'}_2)_2]^{2+}$ systems depend only on the potentials of the $Ni^{II/I}$ and $Ni^{I/0}$ couples and the pK_a values of the protonated primary amine corresponding to the pendant amine in the metal complex. As a result, similar diagrams can be constructed for any catalyst of this class and for any set of catalytic conditions.[94] This permits a systematic search for optimal catalysts and conditions based on the free energies of potential catalytic intermediates, and research in this area is in progress.

Evolution of Ni Catalysts Containing Pendant Amines. The evolution of the Ni pendant amine electrocatalysts for H_2 oxidation and production is illustrated in Scheme 19. Complex $\mathbf{17^{2+}}$ represents a first-generation catalyst for H_2 oxidation, and the use of an exogenous base, such as triethylamine, is required for heterolytic cleavage of H_2. This catalyst is slow (TOF < 0.2 s^{-1} under 1.0 atm of H_2) and exhibits a large OP (1.2 V).[65] The incorporation of a pendant amine to form $\mathbf{18^{2+}}$ results in a much lower OP (0.5 V), but the catalytic rate remains low (TOF < 0.2 s^{-1} under 1.0 atm of H_2 and excess triethylamine to act as a proton acceptor).[65] The incorporation of *positioned* pendant amines in the $[Ni(P^R_2N^{R'}_2)_2]^{2+}$ class of catalysts, e.g., $\mathbf{27^{2+}}$, results in more than 100-fold enhancement in the rates while maintaining a modest OP (0.4 V) under the same conditions.[66,86] By controlling the thermodynamic driving force for H_2 addition to complexes such as $\mathbf{27^{2+}}$ and H_2 elimination from complexes such as $\mathbf{ee28^{2+}}$, it is possible to design catalysts for H_2 production, H_2 oxidation, and reversible H_2 production/oxidation.[66,82,86,91] However, exo protonation and the presence of intraligand NH···N hydrogen bonding lead to bottlenecks in

Scheme 19. Evolution of H_2 Oxidation and Production Catalysts

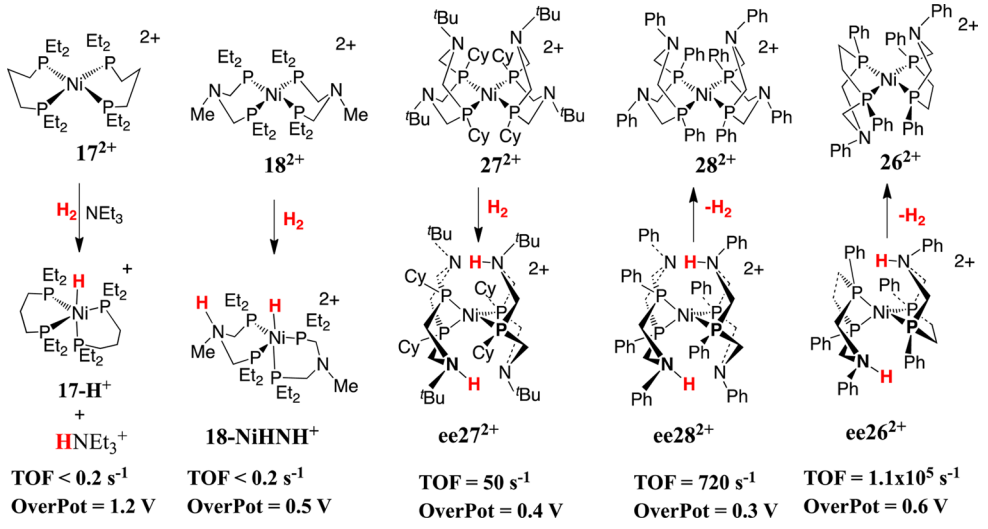

dx.doi.org/10.1021/ic4026969 | Inorg. Chem. 2014, 53, 3935−3960

the catalytic pathways for H_2 production catalysis as discussed above. The $[Ni(7\text{-}P^{Ph}_2N^{Ph})_2]^{2+}$ catalyst, $\mathbf{26}^{2+}$, avoids this intraligand hydrogen bonding, and higher catalytic activities are observed for this complex but also with an increase in the OP.[92,93] This progression of catalysts represents an evolution of the first and second coordination spheres and in the catalyst performance as proton movement is more precisely controlled.

Role of the Outer Coordination Sphere. The preceding discussions have focused primarily on the roles of the first and second coordination spheres in determining the catalyst performance. [FeFe]Hydrogenase enzymes control proton movement between acids and bases in solution and the pendant amine of the second coordination sphere by using proton conduction channels in the outer coordination sphere.[3,4] For $[Ni(P^R_2N^{R'}_2)_2]^{2+}$ catalysts, water enhances catalytic rates from 1.5 to 50 times, and electrochemical, NMR, and computational studies suggest that bridging water molecules facilitate proton transfer between the pendent amine in the second coordination sphere and an acid or base in solution.[80,82] Thus, water is an active component of the outer coordination sphere, reducing the barrier to intermolecular proton transfer.

Protic ionic liquids, such as dibutylformamidium bis(trifluoromethanesulfonyl)amide {[HDBF]N(Tf)$_2$)},[95] offer the possibility of using the solvent to assist in the delivery of protons to a catalyst in a manner similar to that of proton channels in the hydrogenase enzymes. The pK_a value of [HDBF]N(Tf)$_2$) (~6.1 in acetonitrile) closely matches that of the reduced form of the robust $[Ni(P^{Ph}_2N^{Ph}_2)_2]^{2+}$ catalyst. This catalyst was modified with hexyl groups to produce $[Ni(P^{Ph}_2N^{C_6H_4hexyl}_2)_2]^{2+}$ and enhance the solubility in the ionic liquid.[96] This catalytic system has a TOF between 43000 and 53000 s^{-1} in an ionic liquid/water mixture, much faster than the rate of 740 s^{-1} observed in acetonitrile using $[HDMF]^+$ as the acid in the presence of water. This 50-fold increase in the catalytic rate is attributed to the ability of the ionic liquid/water mixture to enhance proton delivery, with the hexyl tail playing an important role in organizing interactions between the acidic solvent and catalyst. Similarly, water is an excellent conductor of protons, which led to the study of $[Ni(P^{Ph}_2N^{C_6H_4OH}_2)_2](BF_4)_2$ in acetonitrile/water mixtures.[97] For this complex, TOFs of 750−170000 s^{-1} were measured at OPs between 310 and 470 mV. These results provide further evidence for an important role of the outer coordination sphere, in this case the solvent/water/catalyst interface, in the delivery of protons.

Shaw and co-workers have undertaken a program that attempts to replicate many of the functional roles performed by the outer coordination sphere of enzymes by attaching amino acids and peptides to the $[Ni(P^R_2N^{R'}_2)_2]^{2+}$ core.[98−100] Attachments of amino acids and dipeptides via meta or para substituents of the NPh group have produced catalysts that are active for H_2 production.[98,99] These studies found that acidic and basic functional groups enhance catalysis by increasing the local concentration of protons around the active site. Another interesting finding is that electron transfer is slower for para-substituted complexes compared to meta-substituted complexes. The latter are thought to have more compact structures, facilitating a closer approach of the catalyst to the electrode and thereby decreasing the barrier for electron transfer.

Attachment of molecular electrocatalysts to electrode surfaces represents another area in which the outer coordination sphere plays an important role in catalyst function. Artero and co-workers have reported the modification of nanotube surfaces with $[Ni(P^R_2N^{R'}_2)_2]^{2+}$ derivatives via covalent attachment through a carboxyl group or via adsorption using pyrene substituents.[101] These surface-immobilized catalysts are active for both H_2 production and oxidation, albeit with lower rates (1−5 s^{-1}) than their solution analogues. One of the pyrene derivatives exhibited a current density of 200 mA/cm^2/mg of catalyst with little or no decomposition over a 10 h test period. In contrast, polymerization of a thiophene derivative of a $[Ni(P^R_2N^{R'}_2)_2]^{2+}$ complex on glassy carbon surface resulted in a complete loss of activity for the immobilized catalyst, possibly because of restriction of the ability of the catalyst to distort from a square-planar to a tetrahedral geometry.[102] These studies clearly indicate that the precise structure of the outer coordination sphere can have major impacts (good and bad) on the catalytic performance.

Importance of Pendant Acids and Bases in the Second Coordination Sphere for Other Electrocatalysts. Control of the proton movement by pendant amines in the second coordination sphere plays an important role in H_2 oxidation and production by the Ni catalysts described above. How general is this observation? Can pendant bases and acids facilitate H_2 oxidation and production for other metal complexes and can pendant acids or bases facilitate electrocatalysis for reactions involving other substrates?

Studies of $[Co(P^R_2N^{R'}_2)(CH_3CN)_3]^{2+}$ complexes indicate that these complexes are catalysts for H_2 production using protonated anilinium acids as a proton source with a TOF of 160 s^{-1} and an OP of 160 mV when R = ^{t}Bu and R′ = Ph.[103] Similarly, $Cp^{C_6F_5}Fe(P^{tBu}_2N^{Bn}_2)H$ and the Mn complex $HMn(P^{Ph}_2N^{Bn}_2)(bppm)(CO)$ [**22-MnH** of Scheme 9, where bppm is $(PAr^F_2)_2CH_2$ and Ar^F = 3,5-bis(trifluoromethyl)-phenyl] also catalyze H_2 oxidation.[72,104] Analogous Co, Fe, and Mn complexes without pendant amines are not active H_2 production or oxidation catalysts. These observations indicate that control of the proton movement provided by the pendant amines plays an important role in catalysis. The common structural feature of these catalysts is the presence of a pendant amine positioned adjacent to a vacant coordination site, a hydride ligand, or an H_2 ligand.

Pendant bases and acids in the second coordination sphere can also facilitate electrocatalytic reactions of other substrates such as O_2, CO_2, and formate. Mayer and co-workers have described an iron porphine catalyst with positioned pendant carboxylic acids that is highly selective for the reduction of O_2 to water in acidic acetonitrile solutions.[105] In addition, X-ray diffraction and NMR studies of Ru complexes clearly demonstrate hydrogen bonding between a protonated pendant amine and a bound O_2 molecule.[106] Nocera and co-workers have developed cobalt porphyrin and corrole catalysts for O_2 reduction containing a pendant carboxylic acid that result in an increase in selectivity to H_2O from 40 to 55% compared to catalysts without the pendant acid.[107] Yang and co-workers described nickel phosphine catalysts with pendant amines in the second coordination sphere that form exclusively H_2O and no H_2O_2, but the ligands are oxidized under catalytic conditions.[108] Very elegant work by Borovik and co-workers describes catalytic O_2 reduction by a Mn complex using a coordinated carboxamide as a proton relay.[109] Savéant and co-workers have shown that a positioned phenolic proton can significantly reduce the OP observed for electrocatalytic reduction of CO_2 to CO.[110] Finally, a pendant base in

dx.doi.org/10.1021/ic4026969 | Inorg. Chem. 2014, 53, 3935−3960

$[NiP^R_2N^{R'}_2)_2]^{2+}$ complexes facilitates the electrocatalytic oxidation of formate to CO_2 by assisting in the removal of a proton from bound formate during a two-electron oxidation of the metal center.[111] These examples, clearly indicate that the introduction of properly positioned bases and acids in the second coordination sphere can result in dramatic beneficial changes in the catalytic activity for different metals and substrates.

SUMMARY AND CONCLUSIONS

A variety of catalysts for each of the reactions shown in Figure 1 will be needed for the electrolysis, photoelectrochemical, and fuel cells associated with the use of renewable energy sources such as solar and wind. Our research has focused on three general themes that could contribute to the rational design of electrocatalysts. The first is the conceptual breakdown of catalysts into first, second, and outer coordination spheres. The second is prediction and control of the energies of catalytic intermediates to avoid high- and low-energy intermediates. The third is precise control of the proton movement over distances of 0.1−10 Å or more.

In our studies of molecular catalysts for CO_2 reduction to CO, the first coordination sphere was optimized in terms of the metal, number of vacant coordination sites, and ligand geometry. This resulted in a new class of electrocatalysts of the general formula [Pd(triphosphine)(solvent)]$^{2+}$ that exhibit attractive properties in terms of rates, OPs, and stability. Significant conclusions are that cleavage of the C−O bond is facilitated by a vacant coordination site and that the structure of the tridentate phosphine ligand determines the rate of CO_2 binding and catalysis. Building on the basic structure of the first coordination sphere, a second coordination sphere was introduced with the objective of stabilizing CO_2 binding and accelerating catalysis without increasing the OP. This research resulted in very fast catalysts for CO_2 reduction with second-order rate constants greater than 25×10^3 M^{-1} s^{-1}, as represented by complex **7**. However, this bimolecular catalyst exhibits a low TON. Thus, the modular approach proved very useful in the discovery and initial optimization of a new class of molecular electrocatalysts for CO_2 reduction, but much remains to be done to realize their full potential.

The second theme of our research, the ability to predict and control the energies of catalytic intermediates, began with measurements of thermodynamic hydride donor abilities (hydricities), and a hydride donor scale was developed for a broad range of organic and organometallic hydrides. These studies were extended to include measurements of pK_a values of metal hydrides, redox potentials, and homolytic bond dissociation free energies to produce much more complete sets of thermodynamic data from which comprehensive thermodynamic diagrams were constructed. A model was developed that allows the prediction of complete sets of thermodynamic parameters for different [Ni(diphosphine)$_2$]$^{2+}$ from a knowledge of the $Ni^{II/I}$ and $Ni^{I/0}$ redox potentials. This predictive approach was extended to the $[Ni(P^R_2N^{R'}_2)_2]^{2+}$ systems by taking into account the pK_a values of the protonated form of the primary amine from which the ligand is derived. These thermodynamic models are powerful tools for understanding and predicting stoichiometric as well as electrocatalytic reactions.

The introduction of pendant amines in the second coordination sphere to control proton movement over a range of distances results in many new possible catalytic pathways. Our studies of $[Ni(P^R_2N^{R'}_2)_2]^{2+}$ complexes indicate that pendant amines in the second coordination sphere can facilitate (1) heterolytic H_2 cleavage/formation, (2) intramolecular proton transfer, (3) intermolecular proton transfer, and (4) the coupling of intra- and intermolecular proton-transfer reactions with electron-transfer reactions. Catalysts containing pendant amines exhibit much lower OPs and much higher catalytic rates than analogous complexes without pendant amines. Recent studies also suggest an important role for the outer coordination sphere in controlling proton movement important for catalysis. In particular, the outer coordination sphere must control the delivery of protons to endo positions to obtain optimal catalyst performance.

The concepts and approaches outlined in this perspective appear to be general. The modular approach to catalyst design, determination and control of the energies of reaction intermediates, and control of the proton movement by pendant acids and bases have been shown to aid the development of electrocatalysts for a variety of substrates using a variety of catalytic platforms. Hopefully, application of these concepts and those developed in other laboratories[6,112] will lead to the future development of fast, efficient, and durable electrocatalysts for the interconversion of electrical and chemical energy in the form of fuels.

AUTHOR INFORMATION

Corresponding Author

*E-mail: daniel.dubois@pnnl.gov.

Notes

The authors declare no competing financial interest.

Biography

Daniel L. DuBois received his B.A. degree from the University of Indianapolis in 1971 and his Ph.D. degree in inorganic chemistry from The Ohio State University in 1975 under the guidance of Devon Meek. He completed postdoctoral studies with Roald Hoffmann at Cornell University, with Gareth Eaton at the University of Denver, and with James C. Smart at the National Renewable Energy Laboratory. He joined the National Renewable Energy Laboratory as a research scientist in 1981, where he led the molecular catalysis team from 1985 through 2005. In 2006, he moved to Pacific Northwest National Laboratory, where he is currently a Laboratory Fellow. In 2010, he was the recipient of the Laboratory's Award for Exceptional Scientific Achievement. His research interests include the catalytic interconversion of fuels and electricity, synthetic organometallic and inorganic chemistry, and thermodynamic studies relevant to catalysis. His research team has developed new electrochemical methods for CO_2

dx.doi.org/10.1021/ic4026969 | Inorg. Chem. 2014, 53, 3935−3960

recovery and new classes of electrocatalysts for CO_2 reduction, hydrogen oxidation, hydrogen production, O_2 reduction, and formate oxidation. His research has also involved accurate thermodynamic measurements of transition-metal hydrides, critical intermediates in a wide range of catalytic reactions. Studies of proton relays have demonstrated their importance and broad utility in a variety of electrocatalytic reactions.

■ ACKNOWLEDGMENTS

D.L.D. acknowledges enjoyable and productive collaborations over many years with his colleagues Mary Rakowski DuBois, R. Morris Bullock, and Calvin J. Curtis. He also thanks other collaborators, students, and postdocs who have contributed to the research described in this manuscript: Alex Miedaner, William Bell, John Linehan, Jim Franz, Michel Dupuis, Wendy Shaw, Aaron Appel, Jenny Yang, John Roberts, Mike Mock, Simone Raugei, Roger Rousseau, Molly O'Hagan, Monte Helm, Eric Wiedner, Dan Blake, Mark Nimlos, Carl Koval, Rich Noble, Arlie Norman, John Bercaw, Jay Labinger, Dorothy Gibson, Jim Muckerman, Etsuko Fujita, Cliff Kubiak, Rebecca Ciancanelli, Renee Henry, Aaron Wilson, George Jacobsen, Rachel Newell, Kendra Fraze, Aaron Appel, Stuart Smith, Uriah Kilgore, Doug Pool, Michael Stuart, Shentan Chen, Ming-Hsun Ho, Tianbio Liu, Brandon Galan, Brian Boro, Andy Herring, Paul Bernatis, Doug Berning, Paul Scovazzo, Sherry Wander, Bryan Steffey, Andrew Price, Jim Raebiger, Wallace Ellis, Stefan Weise, Charles Weiss, Jonathan Darmon, Ming Fang, Zachariah Heiden, Elliott Hulley, Wesley Hoffert, and Michael Stewart. Funding for the research described in this manuscript was provided as part of the Center for Molecular Electrocatalysis, an Energy Frontier Research Center supported by the U.S. Department of Energy, Office of Science, and through individual grants from the Office of Science, Office of Basic Energy Sciences, Division of Chemical Sciences, Biosciences, and Geosciences. Pacific Northwest National Laboratory is operated by Battelle for the U.S. Department of Energy.

■ REFERENCES

(1) Cook, T. R.; Dogutan, D. K.; Reece, S. Y.; Surendranath, Y.; Teets, T. S.; Nocera, D. G. *Chem. Rev.* **2010**, *110*, 6474−6502.
(2) Karlin, S.; Zhu, Z.-Y.; Karlin, K. D. *Proc. Natl. Acad. Sci. U.S.A.* **1997**, *94*, 14225−14230.
(3) (a) Nicolet, Y.; Piras, C.; Legrand, P.; Hatchikian, C. E.; Fontecilla-Camps, J. C. *Structure* **1999**, *7*, 13−23. (b) Nicolet, Y.; de Lacey, A. L.; Vernède, X.; Fernandez, V. M.; Hatchikian, E. C.; Fontecilla-Camps, J. C. *J. Am. Chem. Soc.* **2001**, *123*, 1596−1601. (c) Silakov, A.; Wenk, B.; Reijerse, E.; Lubitz, W. *Phys. Chem. Chem. Phys.* **2009**, *11*, 6592−6599. (d) Peters, J. W.; Lanzilotta, W. N.; Lemon, B. J.; Seefeldt, L. C. *Science* **1998**, *282*, 1853−1858. (e) Volbeda, A.; Fontecilla-Camps, J. C. *J. Chem. Soc., Dalton Trans.* **2003**, 4030−4038. (f) Frey, M. *ChemBioChem* **2002**, *3*, 153−160.
(4) (a) Williams, R. J. P. *Nature* **1995**, *376*, 643. (b) Montet, Y.; Amara, P.; Volbeda, A.; Vernède, X.; Hatchikian, E. C.; Field, M. J.; Frey, M.; Fontecilla-Camps, J. C. *Nat. Struct. Biol.* **1997**, *4*, 523.
(5) (a) Figueroa, J. D.; Fout, T.; Plasynski, S.; McIlvried, H.; Srivastava, R. D. *Int. J. Greenhouse Gas Control* **2008**, *2*, 9−20. (b) Lackner, K. S. *Energy Proc.* **2011**, *4*, 2869−2876. (c) Eisaman, M. D.; Alvarado, L.; Larner, D.; Wang, P.; Garg, B.; Littau, K. A. *Energy Environ. Sci.* **2011**, *4*, 1319−1328. (d) Bandi, A.; Specht, M.; Weimer, T.; Schaber, K. *Energy Convers. Manage.* **1995**, *36*, 899−902.
(6) (a) Appel, A. M.; Bercaw, J. E.; Bocarsly, A. B.; Dobbek, H.; DuBois, D. L.; Dupuis, M.; Ferry, J. G.; Fujita, E.; Hille, R.; Kenis, P. J. A.; Kerfeld, C. A.; Morris, R. H.; Peden, C. H. F.; Portis, A. R.; Ragsdale, S. W.; Rauchfuss, T. B.; Reek, J. N. H.; Seefeldt, L. C.; Thauer, R. K.; Waldrop, G. L. *Chem. Rev.* **2013**, *113*, 6621−6658. (b) Benson, E. E.; Kubiak, C. P.; Sathrum, A. J.; Smieja, J. M. *Chem. Soc. Rev.* **2009**, *38*, 89−99. (c) Savéant, J. M. *Chem. Rev.* **2008**, *108*, 2348−2378. (d) Schneider, J.; Jia, H.; Muckerman, J. T.; Fujita, E. *Chem. Soc. Rev.* **2012**, *41*, 2036−2051. (e) DuBois, D. L. *Encycl. Electrochem.* **2006**, *7a*, 202−225.
(7) (a) Scovazzo, P.; Poshusta, J.; DuBois, D. L.; Koval, C. A.; Noble, R. D. *J. Electrochem. Soc.* **2003**, *150*, D91−D98. (b) Bell,W. L.; Miedaner, A.; Smart, J. C.; DuBois, D. L.; Verostko, C. E. Society of Automotive Engineers Technical Paper Series No. 881078, 1988. (c) Appel, A. M.; Newell, R.; DuBois, D. L.; Rakowski DuBois, M. *Inorg. Chem.* **2005**, *44*, 3046−3056.
(8) DuBois, D. L.; Miedaner, A. *Inorg. Chem.* **1986**, *25*, 4642−4650.
(9) DuBois, D. L.; Miedaner, A. *J. Am. Chem. Soc.* **1987**, *109*, 113.
(10) DuBois, D. L.; Miedaner, A. *Adv. Chem. Ser.* **1988**, *363*, 42.
(11) (a) Fisher, B. J.; Eisenberg, R. *J. Am. Chem. Soc.* **1980**, *102*, 7361−7363. (b) Beley, M.; Collin, J. P.; Ruppert, R.; Sauvage, J. P. *J. Am. Chem. Soc.* **1986**, *108*, 7461−7467. (c) Fachinetti, G.; Floriani, C.; Zanazzi, P. F. *J. Am. Chem. Soc.* **1978**, *100*, 7405−7407. (d) Pearce, D. J.; Pletcher, D. *J. Electroanal. Chem. Interfacial Electrochem.* **1986**, *197*, 317−330. (e) Creutz, C. In *Electrochemical and Electrocatalytic Reactions of Carbon Dioxide*; Sullivan, B. P., Krist, K., Guard, H. E., Eds.; Elsevier: New York, 1993; Chapter 2. (f) Takeuchi, K. J.; Thompson, M. S.; Pipes, D. W.; Meyer, T. J. *Inorg. Chem.* **1984**, *23*, 1845. (g) Bolinger, C. M.; Story, N.; Sullivan, B. P.; Meyer, T. J. *Inorg. Chem.* **1988**, *27*, 4582−4587.
(12) Darensbourg, D. J.; Darensbourg, M. Y.; Goh, L. Y.; Ludvig, M.; Wiegreffe, P. *J. Am. Chem. Soc.* **1987**, *109*, 7539−7540.
(13) Slater, S.; Wagenknecht, J. H. *J. Am. Chem. Soc.* **1984**, *106*, 5367−5368.
(14) (a) DuBois, D. L.; Haltiwanger, R. C.; Miedaner, A. *J. Am. Chem. Soc.* **1991**, *114*, 8753−8764. (b) Bernatis, P. R.; Curtis, C. J.; Herring, A.; Miedaner, A.; DuBois, D. L. *The International Symposium on Chemical Fixation of Carbon Dioxide*, Nagoya, Japan, 1991; pp 89−96.
(15) Bernatis, P. R.; Miedaner, A.; Haltiwanger, R. C.; DuBois, D. L. *Organometallics* **1994**, *13*, 4835−4843.
(16) Steffey, B. D.; Miedaner, A.; Maciejewski-Farmer, M. L.; Bernatis, P. R.; Herring, A. M.; Allured, V.; Carperos, V.; DuBois, D. L. *Organometallics* **1994**, *13*, 4844−4855.
(17) Wander, S. A.; Miedaner, A.; Noll, B. C.; DuBois, D. L. *Organometallics* **1996**, *15*, 3360.
(18) Herring, A. M.; Steffey, B. D.; Miedaner, A.; Wander, S. A.; DuBois, D. L. *Inorg. Chem.* **1995**, *34*, 1100−1109.
(19) Raebiger, J. W.; Turner, J. W.; Noll, B. C.; Curtis, C. J.; Miedaner, A.; Cox, B.; DuBois, D. L. *Organometallics* **2006**, *25*, 3345−3351.
(20) Miedaner, A.; Noll, B. C.; DuBois, D. L. *Organometallics* **1997**, *16*, 5779−5791.
(21) Steffey, B. D.; Curtis, C. J.; DuBois, D. L. *Organometallics* **1995**, *14*, 4937−4943.
(22) (a) Svetlitchnyi, V.; Peschel, C.; Acker, G.; Meyer, O. *J. Bacteriol.* **2001**, *183*, 5134−5144. (b) Ensign, S. A.; Bonam, D.; Ludden, P. W. *Biochemistry* **1989**, *28*, 4968−73. (c) Ragsdale, S. W.; Clark, J. E.; Ljungdahl, L. G.; Lundie, L. L.; Drake, H. L. *J. Biol. Chem.* **1983**, *258*, 2364−2369.
(23) Jeoung, J.-H.; Dobbek, H. *Science* **2007**, *318*, 1461−1464.
(24) Darnault, C.; Volbeda, A.; Kim, E. J.; Legrand, P.; Vernede, X.; Lindahl, P. A.; Fontecilla-Camps, J. C. *Nat. Struct. Biol.* **2003**, *10*, 271−279.
(25) Miedaner, A.; Curtis, C. J.; Barkley, R. M.; DuBois, D. L. *Inorg. Chem.* **1994**, *33*, 5482−5490.
(26) (a) DuBois, D. L. *Advances in Chemical Conversions for Mitigating Carbon Dioxide*; Studies in Surface Science and Catalysis; Elsevier Science: New York, 1998; Vol. *114*, pp 43−53. (b) DuBois, D. L. *Comments Inorg. Chem.* **1997**, *19*, 307. (c) Rakowski DuBois, M.; DuBois, D. L. *Acc. Chem. Res.* **2009**, *42*, 1974−1982.
(27) (a) Yang, Z.-Y.; Dean, D. R.; Seefeldt, L. C. *J. Biol. Chem.* **2011**, *286*, 19417−19421. (b) Hu, Y.; Lee, C. C.; Ribbe, M. W. *Science* **2011**,

333, 753−755. (c) Lee, C. C.; Hu, Y.; Ribbe, M. W. *Angew. Chem., Int. Ed.* **2012**, *51*, 1947−1949.
(28) (a) Casey, C. P.; Andrews, M. A.; McAlister, D. R.; Rinz, J. E. *J. Am. Chem. Soc.* **1980**, *102*, 1927−1933. (b) Sweet, J. R.; Graham, W. A. G. *J. Am. Chem. Soc.* **1982**, *104*, 2811−2815. (c) Tam, W.; Lin, G.-Y.; Wong, W.-K.; Kiel, W. A.; Wong, V. K.; Gladysz, J. A. *J. Am. Chem. Soc.* **1982**, *104*, 141−152. (d) Gibson, D. H.; Owens, K.; Mandal, S. K.; Sattich, W. E.; Franco, J. O. *Organometallics* **1989**, *8*, 498−505. (e) Tam, W.; Wong, W.-K.; Gladysz, J. A. *J. Am. Chem. Soc.* **1979**, *101*, 1589−1591.
(29) Miedaner, A.; DuBois, D. L.; Curtis, C. J.; Haltiwanger, R. C. *Organometallics* **1993**, *12*, 299−303.
(30) (a) Labinger, J. A. In *Transition Metal Hydrides: Recent Advances in Theory and Experiment*; Dedieu, A., Ed.; VCH: New York, 1991; pp 361−379. (b) Labinger, J. A.; Komadina, K. H. *J. Organomet. Chem.* **1978**, *155*, C25−C28. (c) Kao, S. C.; Spillett, C. T.; Ash, C.; Lusk, R.; Park, Y. K.; Darensbourg, M. Y. *Organometallics* **1985**, *4*, 83−91. (d) Kao, S. C.; Gaus, P. L.; Youngdahl, K.; Darensbourg, M. Y. *Organometallics* **1984**, *3*, 1601−1603. (e) Gaus, P. L.; Kao, S. C.; Youngdahl, K.; Darensbourg, M. Y. *J. Am. Chem. Soc.* **1985**, *107*, 2428−2434. (f) Darensbourg, M. Y.; Ash, C. E. *Adv. Organomet. Chem.* **1987**, *27*, 1−50. (g) Kinney, R. J.; Jones, W. D.; Bergman, R. G. *J. Am. Chem. Soc.* **1978**, *100*, 7902−7915. (h) Martin, B. D.; Warner, K. E.; Norton, J. R. *J. Am. Chem. Soc.* **1986**, *108*, 33−39. (i) Hembre, R. T.; McQueen, J. S. *Angew. Chem., Int. Ed. Engl.* **1997**, *36*, 65−67. (j) Hembre, R. T.; McQueen, S. *J. Am. Chem. Soc.* **1994**, *116*, 2141−2142. (k) Cheng, T.-Y.; Brunschwig, B. S.; Bullock, R. M. *J. Am. Chem. Soc.* **1998**, *120*, 13121−13137.
(31) Berning, D. E.; Noll, B. C.; DuBois, D. L. *J. Am. Chem. Soc.* **1999**, *121*, 11432−11447.
(32) Cheng, J.-P.; Handoo, K. L.; Xue, J.; Parker, V. D. *J. Org. Chem.* **1993**, *58*, 5050−5054.
(33) Wayner, D. D. M.; Parker, V. D. *Acc. Chem. Res.* **1993**, *26*, 287−294.
(34) (a) Kaljurand, I.; Rodima, T.; Leito, I.; Koppel, I. A.; Schwesinger, R. *J. Org. Chem.* **2000**, *65*, 6202−6208. (b) Kaljurand, I.; Kütt, A.; Sooväli, L.; Rodima, T.; Mäemets, V.; Leito, I.; Koppel, I. *J. Org. Chem.* **2005**, *70*, 1019−1028. (c) Kütt, A.; Leito, I.; Kaljurand, I.; Sooväli, L.; Vlasov, V. M.; Yagupolskii, L. M.; Koppel, I. *J. Org. Chem.* **2006**, *71*, 2829−2838. (d) Li, T.; Lough, A. J.; Morris, R. H. *Chem.—Eur. J.* **2007**, *13*, 3796−3803.
(35) Curtis, C. J.; Miedaner, A.; Ellis, W. W.; DuBois, D. L. *J. Am. Chem. Soc.* **2002**, *124*, 1918−1925.
(36) Ellis, W. W.; Miedaner, A.; Gibson, D. H.; Curtis, C. J.; DuBois, D. L. *J. Am. Chem. Soc.* **2002**, *124*, 1926−1932.
(37) Ellis, W. W.; Raebiger, J. W.; Curtis, C. J.; Bruno, J. W.; DuBois, D. L. *J. Am. Chem. Soc.* **2004**, *126*, 2738−2743.
(38) DuBois, D. L.; Blake, D. M.; Miedaner, A.; Curtis, C. J.; Rakowski DuBois, M.; Franz, J. A.; Linehan, J. C. *Organometallics* **2006**, *25*, 4414−4419.
(39) Mock, M. T.; Potter, R. G.; Camaioni, D. M.; Li, J.; Dougherty, W. G.; Kassel, W. S.; Twamley, B.; DuBois, D. L. *J. Am. Chem. Soc.* **2009**, *131*, 14454−14465.
(40) (a) Handoo, K. L.; Cheng, J.-P.; Parker, V. D. *J. Am. Chem. Soc.* **1993**, *115*, 5067−5072. (b) Zhang, X.-M.; Bruno, J. W.; Ennyinnaya, E. *J. Org. Chem.* **1998**, *63*, 4671−4678.
(41) Larsen, A. S.; Wang, K.; Lockwood, M. A.; Rice, G. L.; Won, T.-J.; Lovell, S.; Sadílek, M.; Turcek, F.; Mayer, J. M. *J. Am. Chem. Soc.* **2002**, *124*, 10112−10123.
(42) (a) Anne, A.; Moiroux, J. *J. Org. Chem.* **1990**, *55*, 4608−4614. (b) Ostovic, D.; Lee, I. S. H.; Roberts, R. M. G.; Kreevoy, M. M. *J. Org. Chem.* **1985**, *50*, 4206−4211.
(43) (a) Appel, A. M.; Lee, S.-J.; Franz, J. A.; DuBois, D. L.; Rakowski DuBois, M. *J. Am. Chem. Soc.* **2009**, *131*, 5224−5232. (b) Appel, A. M.; Lee, S.-J.; Franz, J. A.; DuBois, D. L.; Rakowski DuBois, M.; Birnbaum, J. C.; Twamley, B. *J. Am. Chem. Soc.* **2008**, *130*, 8940−8951.
(44) Ellis, W. W.; Ciancanelli, R.; Miller, S. M.; Raebiger, J. W.; Rakowski DuBois, M.; DuBois, D. L. *J. Am. Chem. Soc.* **2003**, *125*, 12230−12236.
(45) Roberts, J. A. S.; Appel, A. M.; DuBois, D. L.; Bullock, R. M. *J. Am. Chem. Soc.* **2011**, *133*, 14604−14613.
(46) Ciancanelli, R. F.; Noll, B. C.; DuBois, D. L.; Rakowski DuBois, M. *J. Am. Chem. Soc.* **2002**, *124*, 2984−2992.
(47) Price, A. J.; Ciancanelli, R.; Noll, B. C.; Curtis, C. J.; DuBois, D. L.; Rakowski DuBois, M. *Organometallics* **2002**, *21*, 4833−4839.
(48) Curtis, C. J.; Miedaner, A.; Raebiger, J. W.; DuBois, D. L. *Orgnometallics* **2004**, *23*, 511−516.
(49) Raebiger, J. W.; Miedaner, A.; Curtis, C. J.; Miller, S. M.; DuBois, D. L. *J. Am. Chem. Soc.* **2004**, *126*, 5502−5514.
(50) Miedaner, A.; Raebiger, J. W.; Curtis, C. J.; Miller, S. M.; DuBois, D. L. *Organometallics* **2004**, *23*, 2670−2679.
(51) Raebiger, J. W.; DuBois, D. L. *Organometallics* **2005**, *24*, 110−118.
(52) Fraze, K.; Wilson, A. D.; Appel, A. M.; Rakowski DuBois, M.; DuBois, D. L. *Organometallics* **2007**, *26*, 3918−3924.
(53) Wilson, A. D.; Miller, A. J. M.; DuBois, D. L.; Labinger, J. A.; Bercaw, J. E. *Inorg. Chem.* **2010**, *49*, 3918−3926.
(54) Berning, D. E.; Miedaner, A.; Curtis, C. J.; Noll, B. C.; Rakowski DuBois, M.; DuBois, D. L. *Organometallics* **2001**, *20*, 1832−1839.
(55) Chen, S.; Rousseau, R.; Raugei, S.; Dupuis, M.; DuBois, D. L.; Bullock, R. M. *Organometallics* **2011**, *30*, 6108−6118.
(56) (a) Miedaner, A.; Haltiwanger, R. C.; DuBois, D. L. *Inorg. Chem.* **1991**, *30*, 417−427. (b) Nimlos, M. R.; Chang, C. H.; Curtis, C. J.; Miedaner, A.; Pilath, H. M.; DuBois, D. L. *Organometallics* **2008**, *27*, 2715−2722.
(57) Kovacs, G.; Papai, I. *Organometallics* **2006**, *25*, 820−825.
(58) Qi, X. J.; Fu, Y.; Liu, L.; Guo, Q. X. *Organometallics* **2007**, *26*, 4197−4203.
(59) Mock, M. T.; Potter, R. G.; O'Hagan, M. J.; Camaioni, D. M.; Dougherty, W. G.; Kassel, W. S.; DuBois, D. L. *Inorg. Chem.* **2011**, *50*, 11914−11928.
(60) Niu, S.; Thomson, L. M.; Hall, M. B. *J. Am. Chem. Soc.* **1999**, *121*, 4000−4007.
(61) (a) Lough, A. J.; Park, S.; Ramachandran, R.; Morris, R. H. *J. Am. Chem. Soc.* **1994**, *116*, 8356−8357. (b) Park, S.; Lough, A. J.; Morris, R. H. *Inorg. Chem.* **1996**, *35*, 3001−3006. (c) Xu, W.; Lough, A. J.; Morris, R. H. *Inorg. Chem.* **1996**, *35*, 1549−1555.
(62) (a) Lee, D.-H.; Patel, B. P.; Clot, E.; Eisenstein, O.; Crabtree, R. H. *Chem. Commun.* **1999**, 297−298. (b) Crabtree, R. H.; Siegbahn, P. E. M.; Eisenstein, O.; Rheingold, A. L.; Koetzle, T. F. *Acc. Chem. Res.* **1996**, *29*, 348−354.
(63) Chu, H. S.; Lau, C. P.; Wong, K. Y.; Wong, W. T. *Organometallics* **1998**, *17*, 2768−2777.
(64) Caballero, A.; Jalón, F. A.; Manzano, B. R. *Chem. Commun.* **1998**, 1879.
(65) Curtis, C. J.; Miedaner, A.; Ciancanelli, R. F.; Ellis, W. W.; Noll, B. C.; Rakowski DuBois, M.; DuBois, D. L. *Inorg. Chem.* **2003**, *42*, 216−227.
(66) Wilson, A. D.; Newell, R. H.; McNevin, M. J.; Muckerman, J. T.; Rakowski DuBois, M.; DuBois, D. L. *J. Am. Chem. Soc.* **2006**, *128*, 358−366.
(67) Wilson, A. D.; Shoemaker, R. K.; Meidaner, A.; Muckerman, J. T.; Rakowski DuBois, M.; DuBois, D. L. *Proc. Natl. Acad. Sci. U.S.A.* **2007**, *104*, 6951−6956.
(68) Yang, J. Y.; Bullock, R. M.; Shaw, W. J.; Twamley, B.; Fraze, K.; Rakowski DuBois, M.; DuBois, D. L. *J. Am. Chem. Soc.* **2009**, *131*, 5935−5945.
(69) Dupuis, M.; Chen, S.; Raugei, S.; DuBois, D. L.; Bullock, R. M. *J. Phys. Chem. A* **2011**, *115*, 4861−4865.
(70) Raugei, S.; Chen, S.; Ho, M.-S.; Ginovska-Pangovska, B.; Rousseau, R. J.; Dupuis, M.; DuBois, D. L.; Bullock, R. M. *Chem.—Eur. J.* **2012**, *18*, 6493−6506.
(71) Welch, K. D.; Dougherty, W. D.; Kassel, W. S.; DuBois, D. L.; Bullock, R. M. *Organometallics* **2010**, *29*, 4532−4540.
(72) Hulley, E. B.; Welch, K. D.; Appel, A. M.; DuBois, D. L.; Bullock, R. M. *J. Am. Chem. Soc.* **2013**, *135*, 11736−11739.
(73) Small, Y. A.; DuBois, D. L.; Fujita, E.; Muckerman, J. T. *Energy Environ. Sci.* **2011**, *4*, 3008.

(74) O'Hagan, M. J.; Shaw, W. J.; Raugei, S.; Chen, S.; Yang, J. Y.; Kilgore, U. J.; DuBois, D. L.; Bullock, R. M. *J. Am. Chem. Soc.* **2011**, *133*, 14151−14468.
(75) (a) King, W. A.; Luo, X.-L.; Scott, B. L.; Kubas, G. J.; Zilm, K. W. *J. Am. Chem. Soc.* **1996**, *118*, 6782−6783. (b) King, W. A.; Scott, B. L.; Eckert, J.; Kubas, G. J. *Inorg. Chem.* **1999**, *38*, 1069−1084.
(76) He, T.; Tsvetkov, N. P.; Andino, J. G.; Gao, X.; Fullmer, B. C.; Caulton, K. G. *J. Am. Chem. Soc.* **2010**, *132*, 910−911.
(77) Liu, T.; Chen, S.; O'Hagan, M. J.; Rakowski DuBois, M.; Bullock, R. M.; DuBois, D. L. *J. Am. Chem. Soc.* **2012**, *134*, 6257−6272.
(78) Henry, R. M.; Shoemaker, R. K.; DuBois, D. L.; Rakowski DuBois, M. *J. Am. Chem. Soc.* **2006**, *128*, 3002−3010.
(79) Jacobsen, G. M.; Shoemaker, R. K.; Rakowski DuBois, M.; DuBois, D. L. *Organometallics* **2007**, *26*, 4964−4971.
(80) O'Hagan, M.; Ho, M.-S.; Yang, J. Y.; Appel, A. M.; Rakowski DuBois, M.; Raugei, S.; Shaw, W. J.; DuBois, D. L.; Bullock, R. M. *J. Am. Chem. Soc.* **2012**, *134*, 19409−19424.
(81) Wiedner, E. S.; Yang, J. Y.; Chen, S.; Raugei, S.; Dougherty, W. G.; Kassel, W. S.; Helm, M. L.; Bullock, R. M.; Rakowski DuBois, M.; DuBois, D. L. *Organometallics* **2012**, *31*, 144−156.
(82) Kilgore, U. J.; Roberts, J. A. S.; Pool, D. H.; Appel, A. M.; Stewart, M. P.; Rakowski DuBois, M.; Dougherty, W. G.; Kassel, W. S.; Bullock, R. M.; DuBois, D. L. *J. Am. Chem. Soc.* **2011**, *133*, 5861−5872.
(83) Darensbourg, D. J.; Robertson, J. B.; Larkins, D. L.; Reibenspies, J. H. *Inorg. Chem.* **1999**, *38*, 2473−2481.
(84) (a) Fernandez, L. E.; Horvath, S.; Hammes-Schiffer, S. *J. Phys. Chem. C* **2012**, *116*, 3171−3180. (b) Horvath, S.; Fernandez, L. E.; Soudackov, A. V.; Hammes-Schiffer, S. *Proc. Natl. Acad. Sci. U.S.A.* **2012**, *109*, 15663−15668.
(85) Franz, J. A.; O'Hagan, M. J.; Ho, M.-S.; Liu, T.; Helm, M. L.; Lense, S.; DuBois, D. L.; Shaw, W. J.; Appel, A. M.; Raugei, S.; Bullock, R. M. *Organometallics* **2013**, *32*, 7034−7042.
(86) Yang, J. Y.; Smith, S. E.; Liu, T.; Dougherty, W. G.; Hoffert, W. A.; Kassel, W. S.; Rakowski DuBois, M.; DuBois, D. L.; Bullock, R. M. *J. Am. Chem. Soc.* **2013**, *135*, 9700−9712.
(87) Wilson, A. D.; Fraze, K.; Twamley, B.; Miller, S. M.; DuBois, D. L.; DuBois, M. R. *J. Am. Chem. Soc.* **2008**, *130*, 1061−1068.
(88) Weise, S.; Kilgore, U. J.; DuBois, D. L.; Bullock, R. M. *ACS Catal.* **2012**, *2*, 720−727.
(89) Kilgore, U. J.; Stewart, M. P.; Helm, M. L.; Dougherty, W. G.; Kassel, W. S.; Rakowski DuBois, M.; DuBois, D. L.; Bullock, R. M. *Inorg. Chem.* **2011**, *50*, 10908−10918.
(90) Appel, A. M.; Pool, D. H.; O'Hagan, M.; Shaw, W. J.; Yang, J. Y.; Rakowski DuBois, M.; DuBois, D. L.; Bullock, R. M. *ACS Catal.* **2011**, *1*, 777−785.
(91) Smith, S. E.; Yang, J. Y.; DuBois, D. L.; Bullock, R. M. *Angew. Chem., Int. Ed.* **2012**, *51*, 3152−3155.
(92) Helm, M. L.; Stewart, M. P.; Bullock, R. M.; Rakowski DuBois, M.; DuBois, D. L. *Science* **2011**, *333*, 863−866.
(93) Stewart, M. P.; Ho, M.-H.; Wiese, S.; Lindstrom, M. L.; Thogerson, C. E.; Raugei, S.; Bullock, R. M.; Helm, M. L. *J. Am. Chem. Soc.* **2013**, *135*, 6033−6046.
(94) Chen, S.; Ho, M.-S.; Bullock, R. M.; DuBois, D. L.; Dupuis, M.; Rousseau, R.; Raugei, S. *ACS Catal.* **2014**, *4*, 229−242.
(95) Huang, J.-F.; Baker, G. A.; Luo, H.; Hong, K.; Li, Q.-F.; Bjerrum, N. J.; Dai, S. *Green Chem.* **2006**, *8*, 599−602.
(96) Pool, D. H.; Stewart, M. P.; O'Hagan, M.; Shaw, W. J.; Roberts, J. A. S.; Bullock, R. M.; DuBois, D. L. *Proc. Natl. Acad. Sci. U.S.A.* **2012**, *109*, 15634−15639.
(97) Hoffert, W. A.; Roberts, J. A. S.; Bullock, R. M.; Helm, M. L. *Chem. Commun.* **2013**, *49*, 7767−7769.
(98) Jain, A.; Reback, M. L.; Lindstrom, M. L.; Thogerson, C. E.; Helm, M. L.; Appel, A. M.; Shaw, W. J. *Inorg. Chem.* **2012**, *51*, 6592−6602.
(99) Lense, S.; Ho, M.-H.; Chen, S.; Jain, A.; Raugei, S.; Linehan, J. C.; Roberts, J. A. S.; Appel, A. M.; Shaw, W. J. *Organometallics* **2012**, *31*, 6719−6731.
(100) (a) Reback, M. L.; Ginovska-Pangovska, B.; Ho, M. H.; Jain, A.; Squier, T. C.; Raugei, S.; Roberts, J. A.; Shaw, W. J. *Chem.—Eur. J.* **2013**, *19*, 1928−1941. (b) Jain, A.; Buchko, G. W.; Reback, M. L.; O'Hagan, M. J.; Ginovska-Pangovska, B.; Linehan, J. C.; Shaw, W. J. *ACS Catal.* **2012**, *2*, 2114−2118. (c) Shaw, W. J. *Catal. Rev.: Sci. Eng.* **2012**, *54*, 489−550.
(101) (a) Le Goff, A.; Artero, V.; Jousselme, B.; Tran, P. D.; Guillet, N.; Métayé, R.; Fihri, A.; Palacin, S.; Fontecave, M. *Science* **2009**, *326*, 1384−1387. (b) Tran, P. D.; Le Goff, A.; Heidkamp, J.; Jousselme, B.; Guillet, N.; Palacin, S.; Dau, H.; Fontecave, M.; Artero, V. *Angew. Chem., Int. Ed.* **2011**, 1371−1374.
(102) Pool, D.; DuBois, D. L. *J. Organomet. Chem.* **2009**, *694*, 2858−2865.
(103) (a) Jacobsen, G. M.; Yang, J. Y.; Twamley, B.; Wilson, A. D.; Bullock, R. M.; Rakowski DuBois, M.; DuBois, D. L. *Energy Environ. Sci.* **2008**, *1*, 167−174. (b) Wiedner, E. S.; Yang, J. Y.; Dougherty, W. G.; Kassel, W. S.; Bullock, R. M.; Rakowski DuBois, M.; DuBois, D. L. *Organometallics* **2010**, *29*, 5390−5401.
(104) Liu, T.; DuBois, D. L.; Bullock, M. R. *Nat. Chem.* **2013**, *5*, 228−233.
(105) Carver, C. T.; Matson, B. D.; Mayer, J. M. *J. Am. Chem. Soc.* **2012**, *134*, 5444−5447.
(106) Tronic, T. A.; Rakowski DuBois, M.; Kaminsky, W.; Coggins, M. K.; Liu, T.; Mayer, J. M. *Angew. Chem., Int. Ed.* **2011**, *50*, 10936−10939.
(107) Dogutan, D. K.; Stoian, S. A.; McGuire, R., Jr.; Schwalbe, M.; Teets, T. S.; Nocera, D. G. *J. Am. Chem. Soc.* **2011**, *133*, 131−140.
(108) Yang, J. Y.; Bullock, R. M.; Doughtery, W. G.; Kassel, W. S.; Twamley, B.; DuBois, D. L.; Rakowski DuBois, M. *Dalton Trans.* **2010**, *39*, 3001−3010.
(109) Shook, R. L.; Peterson, S. M.; Greaves, J.; Moore, C.; Rheingold, A. L.; Borovik, A. S. *J. Am. Chem. Soc.* **2011**, *133*, 5810−5817.
(110) Costentin, C.; Drouet, S.; Robert, M.; Savéant, J.-M. *Science* **2012**, *338*, 90−94.
(111) (a) Galan, B. R.; Schoffel, J.; Linehan, J. C.; Seu, C.; Appel, A. M.; Roberts, J. A.; Helm, M. L.; Kilgore, U. J.; Yang, J. Y.; DuBois, D. L.; Kubiak, C. P. *J. Am. Chem. Soc.* **2011**, *133*, 12767−12779. (b) Seau, C. S.; Appel, A. M.; Doud, M. D.; DuBois, D. L.; Kubiak, C. P. *Energy Environ. Sci.* **2012**, *5*, 6480−6490.
(112) (a) Manor, B. C.; Rauchfuss, T. B. *J. Am. Chem. Soc.* **2013**, *135*, 11895−11900. (b) Camara, J. M.; Rauchfuss, T. B. *Nat. Chem.* **2012**, *4*, 26−30. (c) Hsieh, C.-H.; Erdem, Ö.F.; Harman, S. D.; Singleton, M. L.; Reijerse, E.; Lubitz, W.; Popescu, C. V.; Reibenspies, J. H.; Brothers, S. M.; Hall, M. B.; Darensbourg, M. Y. *J. Am. Chem. Soc.* **2012**, *134*, 13089−13102. (d) Pullen, S.; Fei, H.; Orthaber, A.; Cohen, S.; Ott, S. *J. Am. Chem. Soc.* **2013**, *135*, 16997−17003. (e) Jablonskytė, A.; Wright, J. A.; Fairhurst, S. A.; Peck, J. N. T.; Ibrahim, S. K.; Oganesyan, V. S.; Pickett, C. J. *J. Am. Chem. Soc.* **2011**, *133*, 18606−18609. (f) Wang, M.; Chen, L.; Sun, L. *Energy Environ. Sci.* **2012**, *5*, 6763−6778. (g) Duan, L.; Bozoglian, F.; Mandal, S.; Stewart, B.; Privalov, T.; Llobet, A.; Sun, L. *Nat. Chem.* **2012**, *4*, 418−423. (h) Yandulov, D. V.; Schrock, R. R. *Science* **2003**, *301*, 76−78. (i) Arashiba, K.; Miyake, Y.; Nishibayashi, Y. *Nat. Chem.* **2011**, *3*, 120−125. (j) Anderson, J. S.; Rittle, J.; Peters, J. C. *Nature* **2013**, *501*, 84−88. (k) Rodriguez, M. M.; Bill, E.; Brennessel, W. W.; Holland, P. L. *Science* **2011**, *334*, 780−783. (l) Hoffman, B. M.; Lukoyanov, D.; Dean, D. R.; Seefeldt, L. C. *Acc. Chem. Res.* **2013**, *46*, 587−595.